The Development of Experimental Setup for Various Magneto-Optical Studies

A thesis presented to

the faculty of

the Russ College of Engineering and Technology of Ohio University

In partial fulfillment

of the requirements for the degree

Master of Science

Mohammed N. Bsatee

August 2015

This thesis titled

The Development of Experimental Setup for Various Magneto-Optical Studies

by

MOHAMMED N. BSATEE

has been approved for

the School of Electrical Engineering and Computer Science

and the Russ College of Engineering and Technology by

Wojciech M. Jadwisienczak

Associate Professor of Electrical Engineering and Computer Science

Dennis Irwin

Dean, Russ College of Engineering and Technology

ABSTRACT

BSATEE, MOHAMMED N., M.S., August 2015, Electrical Engineering

The Development of Experimental Setup for Various Magneto-Optical Studies

Director ofThesis: Wojciech M. Jadwisienczak

Progress in modern, widely-defined information technology is strongly determined by the abilities of detailed characterization of semiconductors, phosphors and composite materials in the wide range of anticipated parameters. Traditional electronics use an electron charge as a primary means for information data computing and storage. In contrast, spintronics utilizes the manipulation of an electrons spin which may facilitate opportunities implementing concepts and applications at nanoscale. In order to pursue spintronics realization, novel magnetic materials are required. One way to study magnetic materials is to observe their magneto-optical properties. Through this way, one can study how light interacts with magnetically active materials in the presence of a magnetic field. In general, in this project we are interested in observing the effect of photons electron spin interaction interceded through spin-orbit combination. This MS project targets developing of experimental setup suitable for studying materials in magnetic field strength up to 1.5 Tesla and light probe with photons energies between 4 eV (UV) to 1 eV (NIR) in temperature range from 7 K to 450 K, respectively. In particular, I will demonstrate my efforts on developing, testing and optimization of existing experimental setup for measuring Magneto Optical Kerr Effect (MOKE), Magnetic Circular Dichorism (MCD) and temperature dependent luminescence with magnetic field stimuli (Magneto Optical (MO) effect). Selection of samples were tested using developed apparatus

including semiconductors crystalline GaMnAs (c-GaMnAs), amorphous AlN:Ni (a-AlN:Ni), polycrystalline $KEu(WO_4)_2$ phosphor.

Additionally, this project demonstrates the successful construction and operation of developed magneto-optical characterization facility by measuring MOKE, MCD and magnetic field dependent luminescence for studied materials.

DEDICATION

This work is dedicated to my father; Nadhim Ali, and my mother; Sundus Al Janabi.

ACKNOWLEDGMENTS

First of all, I would like to give my deepest appreciation and sincerest gratitude to Dr. Wojciech M. Jadwisienczak for investing his time in advising and mentoring me throughout this project. Dr. Jadwisienczak has extended this considerable opportunity by including me in a research project of such magnitude which involved working with four different research subjects. Working under the supervision of Dr. Jadwisienczak at Ohio University has further enabled me to utilize my acquired knowledge and experiences in my endeavor to become a successful engineer.

I wish also to extend thanks and express my sincere appreciation to Dr. Savas Kaya, Dr. Faiz Rahman, and Dr. Eric Stinaff for serving as my graduate committee and for offering their critical, yet constructive feedback and suggestions. Furthermore, I thank Dr. H. Saito and Dr. A. Ando of the National Institute of Advanced Industrial Science and Technology (AIST) in Japan for providing research materials for this project. I would like to thank the Department of Electrical engineering and Computer science for providing scholarship during my term at Ohio University. Furthermore, I acknowledge the Nano Quantum Phenomena Institute (NQPI) for assistance in acquiring a necessary hardware for developing experimental setup.

Furthermore, I greatly appreciate the encouragements and the continuous supports from my great friends, Tawny Jones, Hiroki Tanaka, Rami Oran, Ghaith Rawagah, Ahmad Al Hammouri, Husam Abu Hajar, Zeyad Alsaeed, and Stacy Fussner during my graduate study at Ohio University.

Finally, I would like to thank my parents for their boundless love and continuous support throughout my life.

TABLE OF CONTENTS

Page

LIST OF FIGURES

Page

1. INTRODUCTION

The progress in modern, widely-defined information technology is strongly determined by the ability of detailed characterization of various semiconductor materials over a wide range of projected parameters. Typically, current electronics use an electron charge for computing whereas spintronics utilize the manipulation of electrons spin which creates new opportunities for implementing concepts and applications at the nanoscale level. In order to fully understand the field of spintronics, one must first perceive the different magnetic materials that are required. Spintronics can be the new leader in technology; however, it must compete with other efficient and powerful technologies such as complementary metal–oxide–semiconductor (CMOS). The most obvious area in which spintronics might best compete with CMOS at the practical level is in memory [1], especially that the memory hierarchy is currently dominated by CMOS as shown in Figure 1, which illustrates the access times related to different levels of memory. These short access times are the key for allowing spintronics to compete.

A second most appealing aspect of spintronics is the rate at which switching occurs. Devices can potentially operate at the frequencies of atomic processes with switching rates well below a nanosecond, like the tunneling bases spintronics devices. Spintronic switching is achieved through discrete transitions between states [2].

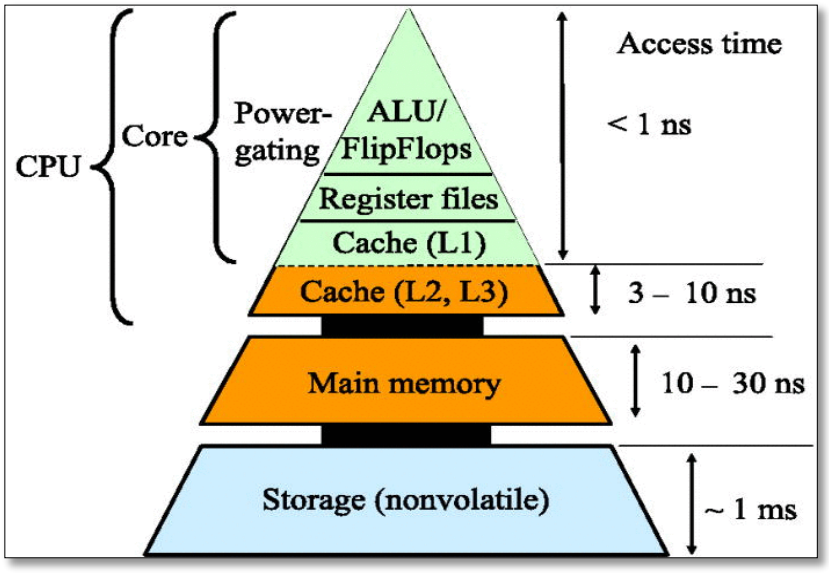

Figure 1 Memory hierarchy in computers. Access times of different levels are shown [1].

The greatest advantage of spintronics in memory storage is that it is non-volatile, meaning the data will continue to be stored with no power input. After only a short energy pulse to perform a switching action, the data can be stored for as long as it is needed. This greatly reduces the amount of energy consumed by spintronics devices [1].

In addition to its non-volatile nature, the ultimate limit of the energy associated with the flipping of spintronic device is low. The limit is being the fine structure splitting in a single atom between nearest states, which is on the order of 10^{-3} eV. Yet, the limit is actually better associated with the typical energy of lattice vibrations at room temperature; 25.6 meV. Any phonons incident on a device that switches with energies near or below this will not be stable at room temperature. Fortunately, as shown in Figure 1, the devices do not need to be completely stable for higher levels in the memory hierarchy. The devices only need to hold their state for nanoseconds. As a result, the energy used to flip the state of a device can be significantly lower than 25.6 meV.

Consequently, materials with magneto-optical properties are those spintronics is focusing on. Thus in order to understand such materials, and to comprehend the spin manipulation in a spintronic material, a magneto optical measurement technique must be performed [3].

Applications such as magneto-optical (MO) storage devices are made possible by magneto-optical spectroscopy. There are many types of magneto-optical spectroscopy, some of which this research has focused on. These include the magneto-optical Kerr effect (MOKE); and magnetic circular dichroism (MCD). Traditionally, magnetic storage is obtained when the magnetic heads in the magnetic recording devices are activated by the induced current due to the changes of the magnetic fluxes on the disk surface [4] . In this case, the magnetic field changes the polarization of the light rather than the current, which is used to store information in the magneto-optical (MO) storage devices [5]. Under the presence of magnetic field, and when the linearly polarized light hits the surface of the magnetic material, the reflected light rotates slightly with respect to the original polarization of the incident light. The reflected light rotates slightly in the reverse direction when the surface magnetization is reversed due to the reversion of the magnetic field. Binary 0 or 1 is determined by the positive or negative orientation of the reflected light from the changes of polarization under the magnetic field in the polar geometry for example [5]. Studying and understanding the magnetic local domain of a specific magnetic material using MOKE has made it feasible because of MOKE's room temperature measurement, sensitivity, simplicity, and relatively low cost [6]. To acquire the strength of a magnetic property of a material; a hysteresis loop must be obtained by

the MOKE technique [5]; which also measures the electron spin orientation in the magnetic materials under the magnetic field. This can be detected when changes in the shape of the hysteresis loop are observed, which brings MOKE technique to the field of spintronics [7]. Spintronics have various applications like the magneto-resistive random access memory (MRAM) [8] and spin transfer switching [9], where the spin of the electron is used instead of the charge. Magneto-Optical spectroscopy is the tool used to test many ferromagnetic materials such as diluted magnetic semiconductors as potential optical and electronic devices.

In the current technological approach, magnetic domains store data as information in the plane of the magnetic material. Large data storage capacity, which is always increasing, requires decreasing size of the magnetic domains. Therefore, reducing the space between the reading/writing head/surface distances is needed [5]. Magneto-optical recording devices can partially solve this problem by focusing a laser beam on domains magnetized perpendicular to the plane. Moreover, the contact between the carrier and the spins gives more flexibility to design new devices. This technology is the latest storage media and it can be defined as the new hybrid read-write technology that offers longer, and more reliable storage than magnetic media [10]. Also, the ferromagnetic semiconductors have been of interest to researchers for being potential nonvolatile transistors [11].

One way to study magnetic materials is to observe their magneto optical properties. Through observation, one can study how light interacts with magnetically active materials in the presence of magnetic field. Specifically, the interest is in observing the

interaction of photons with electron spin interceded with spin-orbit combination [5]. This project targets developing a sensitive experimental setup suitable for studying different materials with magnetic properties using magnetic field strength of up to 1.5 Tesla and light probe with photons energies in the range of 4 eV (UV) to 1 eV (NIR) in a temperature range of 7 K to 450 K; respectively. Therefore; designing, testing, and optimizing the existing Magneto Optical Kerr Effect (MOKE) and Magnetic Circular Dichorism (MCD) setups will be needed to better understand the effect of these materials. Additionally, developing the setup for studying temperature dependent luminescence with magnetic field stimuli (Magneto Optical (MO) effect) is also desirable. Different samples were tested using developed setups including semiconductors GaMnAs, a-AlN:Ni, and wide band gap materials $KEu(WO_4)_2$.

The ultimate goal of this thesis is to demonstrate successful construction and operation of the proposed magneto-optical experimental setup.

2. BACKGROUND

This chapter reviews the developed experimental setups for testing the research samples. The following section describes the different types of magneto-optical effects and selection rules for different materials.

2-1 Types of Magneto-Optical Phenomena

The magneto-optical effect/phenomena is the interaction between magnetic ions and light photons, due to the concept of conservation of angular momentum of the optical selection (transition) rule [12].

This technique is widely used in studying and understanding the optical and the magnetic effect of solid state material. Scientists like Faraday, Zeeman, Voigt, Cotton-Mouton, and Kerr, were the ones that the Magneto-optical spectroscopy technique were named after [5].

In the Faraday effect, and under a strong magnetic field, a linearly polarized light is propagated with a specific angle of incident through a transparent sample. The sample is positioned in the polar geometry, where both the linearly polarized light and the magnetic field are perpendicular to the surface of the sample [13]. The material must have a substantial volume where the linearly polarized light can propagate through as shown in Figure 2.

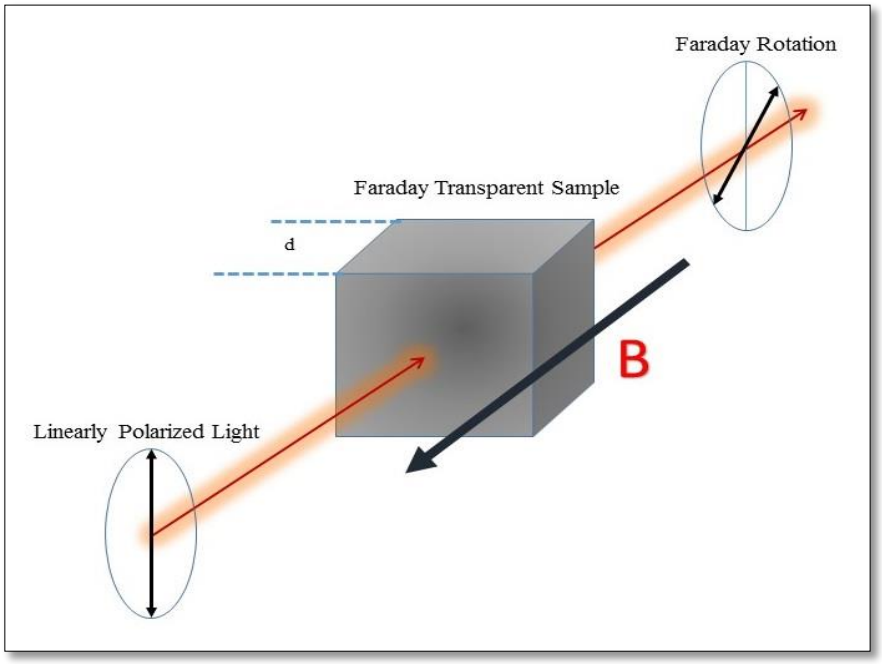

*Figure 2. The Faraday MO experiment, where d is the thickness of the transparent sample, and **B** is the magnetic field.*

In the Zeeman effect, the different levels of the atomic energy level in a semiconductor material can split under the presence of a strong magnetic field, which will result in an increased number of energy levels and spectral line, which will also increase the energy absorbed by the spectrometer. The magnetic field is a result of the splitting in the energy level once the magnetic field is turned off; thus, the material returns to its initial state. Figure 3 illustrates the energy level splitting [3].

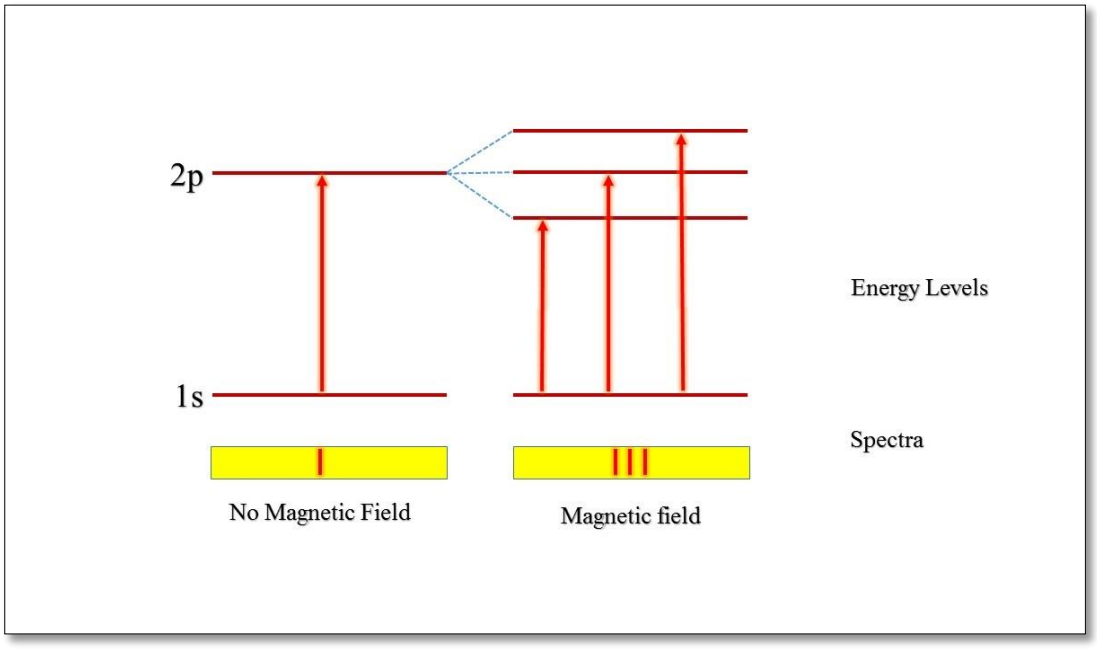

Figure 3. Energy level splitting under magnetic field due to the Zeeman Effect, where 1s, and 2p are the energy levels.

The Voigt and Cotton-Mouton effect share the same light propagation condition as the Faraday effect, but they differ in the magnetic field direction and strength of the effect, where the former is reduced. The Voigt and Cotton-Mouton applies a parallel magnetic field to the sample surface. The noticeable difference between the two is that Voigt effect utilizes a Na vapor whereas Cotton-Mouton uses paramagnetic liquids [14]. Due to the lower effect in solid materials, only few measurements were conducted and reported on the MO effects in known magnetic materials [13].

In the Kerr effect, the magnetic material is excited with a linearly polarized light and a magnetic field. After excitation, an elliptically polarized light is reflected from the sample. Kerr effect is characteristically measured in three different geometries: polar, longitudinal, and transverse. The orientation of the magnetic field with respect to the

orientation of a magnetic sample and the incident plane is what defines these three geometries, which are explained in details in Chapter 3. Figure 4 illustrates the MO Kerr effect.

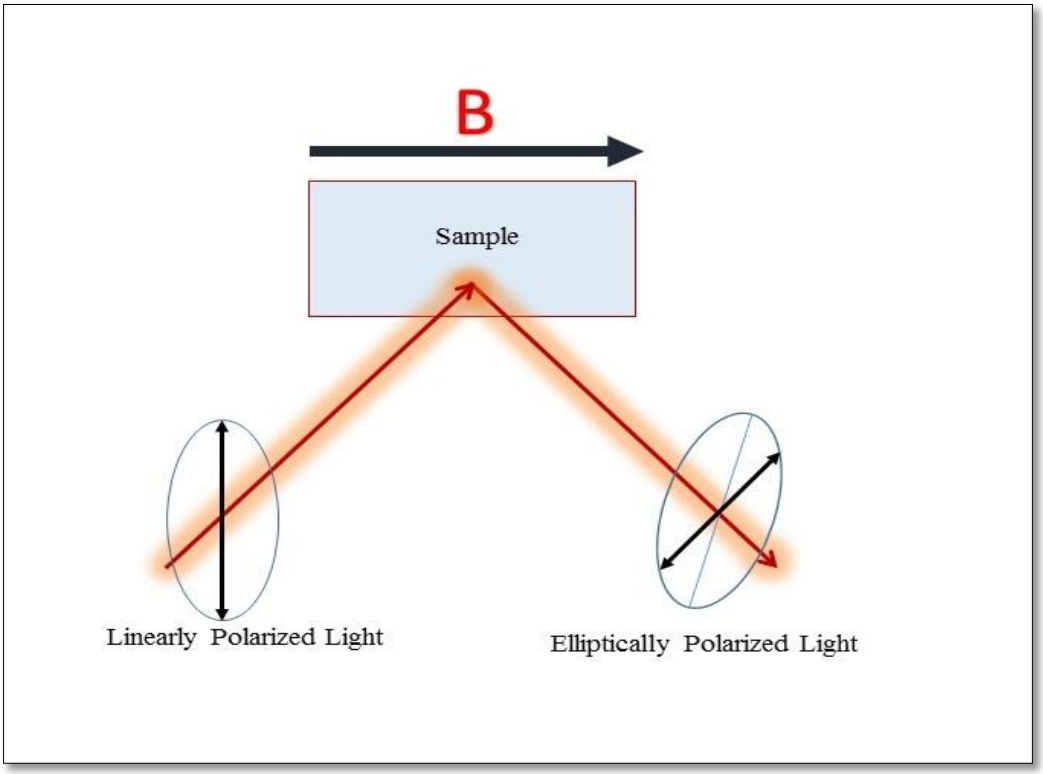

Figure 4. The MO Kerr Effect in the reflection mode.

The material undergoes an anisotropic symmetry and has anisotropic properties when an external force such as an external magnetic field is applied. The light that passes through the material undergoes a double refraction with an optical rotation when the magnetic field re-orients both the magnetic and electric dipoles. To further explain this phenomenon, one must first understand that such an effect is due to the Zeeman splitting in the energy bands, and that when the magnetic field is applied, the electrons' orbitals

are quantized. Therefore, depending on the orientation of the magnetic field direction, the energy of the electron can rotate either clockwise or counter clockwise, and that is when the optical selection rule is observed depending on the polarization of the photons. In the case of MOKE spectroscopy, the linearly polarized light exhibits a rotation in the polarization plane. Whereas in the MCD spectroscopy, the magnetic circular dichroism is obtained when an absorption difference between the left and right circularly polarized light is measured [12]. Such effect in the material is due to its ferromagnetism properties.

2-2 Theoretical Background of the Materials Studied

Typically, ferromagnetic semiconductors are achieved by replacing some of the positive ions in a typical nonmagnetic semiconductor with magnetic ions. This type of material is called a diluted magnetic semiconductor material (DMS). DMSs have magnetic, electronic, and optical properties [15], [16]. Due to having both properties of semiconductors and magnets, it is important to observe their magneto-optical effect, which can be two orders of magnitude larger than that in non-magnetic semiconductors [17]. These properties lead to a wider range of applications like magneto-optic disk memories [18] and optical isolators and circulators for optical communication [19]. Another known application is the Er-doped optical fiber, which was designed by utilizing the Faraday effect of CdHgMnTe DMS as an optical isolator [20]. DMS materials such as GaMnAs, GaN:Mn and InAs:Mn can be used widely in many magneto-optical applications because of their abilities to sustain their magnetic state once magnetized

until the magnetic field is reversed. As a result, a magnetic memory device can be designed based on the ability of attaining a ferromagnetic hysteresis [11].

In order to observe such a magnetic effect, a very sensitive and complicated measurement must be conducted. Measurement techniques like the super conducting quantum interference devices (SQUIDs) are being typically used to detect DMS materials. However, SQUID measurement is a volumetric type measurement and it can detect some other ferromagnetic signals that can interfere with the DMS signal [11]. Therefore, a more precise measurement technique is needed to distinguish the difference in such interference. Magnetic Circular Dichroism (MCD) was introduced to detect the ferromagnetic semiconductor signal. As stated earlier, MCD spectroscopy detects the optical absorption difference between left circularly polarized light and right circularly polarized light on the claimed DMS [11]. Such optical absorption difference comes from the electrons spin polarization of the exchange interaction between the *d*-electrons of the magnetic ions and the *s*-*p*-electrons in the semiconductor material. The obtained MCD signal will have a specific amplitude that is obtained from the magnetic ions and a specific spectra shape that is determined by the semiconductor material due to its band structure [11]. Given the previous facts, one can develop the MCD spectroscopy experimental setup, and measure the MCD signal on GaMnAs DMS samples with different Mn ions concentrations.

The GaMnAs has gained interest due to its prominent properties. GaAs is one of the most well-known and commonly used semiconductor materials, and has a wider band gap (1.42 eV) compared to silicon (1.12 eV), which makes it better for high-temperature

applications. Additionally, it has been used in many applications like Red LED, Red LASERS, and can be used for high electron mobility transistors. Since GaAs has great semiconductor properties, it can be doped with Mn for its great magnetic properties. Mn doping increases the band gap energy (1.52 eV) without changing the band gap structure. Moreover, one can expect great applications such as using DMS material in the spin field effect transistors for more efficient spin injections between the source and drain.

There are other types of Magneto-Optical (MO) effects, but the one that is most relevant to the thesis topic is the effect of the magnetic field on the intensity of the photo luminescence (PL). The external magnetic field can have an effect on the PL intensity of the material, which mainly depends on the type of the material. Rare earth ions (REI) doped phosphors exhibit a memory like MO effect when magnetized, which means that the material keeps its effect even when the magnetic field is turned off. The effect occurs when the materials exhibit a structural phase transition under magnetization and due to the optical selection rule in rare earth ions in crystals [22].

A magneto-optical effect is observed on REI compounds due to the magnetic moment characterization of the ions. The electron spin-related interaction is observed between the ions and the applied external magnetic field [22]. This interaction is due to the ground state electronic configuration which is presented by the unfilled $4f^n$ shell. A splitting in the energy level of the free REI in the $4f^n$ shell is obtained when excited with enough energy. The splitting is presented by the energies at the ground state, ground terms, and the first excited multiplet. In this case, Eu^{3+} has a ground shell configuration on $4f^6$, with

ground term, ground multiplet, and first ground multiplet of ^7F, $^7F_0$, and $^7F_1$, respectively [22]. Figure 5 shows the splitting of the energy levels for the free REI.

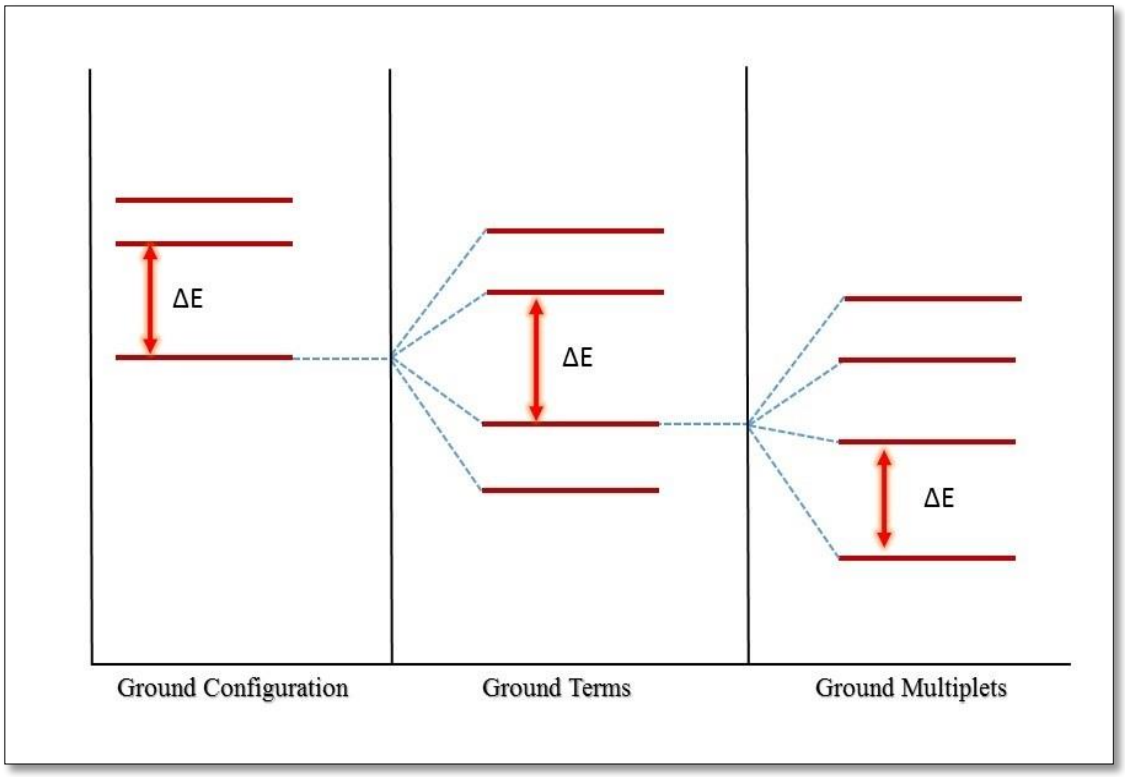

Figure 5. The energy level splitting in the free rare earth ions

The magneto-optical selection rule can be related to the Jahn-Teller effect in rare earth compounds. Jahn-Teller effect, also known as the co-operative Jahn-Teller effect, is a structural phase transition phenomena, which occurs when the localized orbital electronic states interact with the crystal lattice. This interaction leads to lattice distortion accommodated by the splitting of the electronic states. As a result, a strain or a change in the crystal's shape is observed near the low transitional temperature, especially in rare

earth compounds. With the presence of a magnetic field, rare earth compounds exhibit a larger Jahn-Teller phase transitional effect compared to the low temperature effect [23].

The magneto-optical effect of Potassium Europium Double Tungstate ($KEu(WO_4)_2$), exhibits an MO effect as a change in the PL intensity when excited with 405 nm diode laser and a magnetic field strength of up to 1.5 Tesla. Many of the potassium rare earth double tungstate compounds are known for their magnetic and structural phase transition properties, which makes them a great candidate for the new magneto-optical devices. In what follows, the review of literature for the various potassium rare earth double tungstate will be discussed in further details.

The Optical emission of Europium-doped potassium ytterbium tungstate ($Eu:KYb(WO_4)_2$) nanocrystals were observed after being synthesized by the modified Pechini method [24]. The obtained emission lines were defined after being excited with a 532-nm neodymium-doped yttrium aluminum garnet (Nd:YAG) laser. The 617-nm red emission lines were emitted along with different band transition. Those transition bands are known by the electric and magnetic dipoles. The electric dipole exhibits a higher intensity than the magnetic dipole. The ratio of the integral intensity of the electric dipole to that in the magnetic dipole is calculated to study the asymmetry parameter (R). In $Eu:KYb(WO_4)_2$ nanocrystal, the *R* value was around 6 to 7 in room and low temperature, respectively, whereas it was 4 in a bulk material [24].

The magneto optical study of a potassium erbium double tungstate ($KEr(WO_4)_2$) grown by top seeded solution growth (TSSG) has demonstrated the MO effect in the spectral range of 1660-400 nm under magnetic field strength of 70 kOe [25]. The study

has improvised a linear increase of the ($KEr(WO_4)_2$) birefringence with the increase of the magnetic field strength, which was due to the deviation of the magnetic field dependency of REI subsystem magnetization. It has also pointed out that a temperature dependence experiment would cause structural changes in the crystal. However, due to the large distance between the ground and nearest excited energy level in the Er^{3+} ions, it had failed to show any spontaneous structural phase transition.

A 40 Tesla pulse magnetic field was induced on a crystal of potassium yttrium tungstate (KYW) and a crystal of potassium gadolinium tungstate (KGW). The materials were excited with a linearly polarized He-Ne laser [26]. According to [26], a magneto-optical effect was observed after applying the magnetic field. The deviations in the intensities remained for a long time and appeared as if they were irreversible even after switching off the magnetic field. [26] explains that the phenomena of a rapid irreversible spin-dependent physicochemical process under the effect of a magnetic field was due to electron spin reorientation in an ion impurity or lattice defects. The change in the electron structure of the crystal, in which the external magnetic field is present, can be caused by removing the spin forbiddennesses of potential channels, changing the optical properties of the material that depends on the particles' oriented magnetic spin moments.

According to [27], an irreversible transformation in the elastic strain of the potassium dysprosium tungstate ($KDy(WO_4)_2$) occurs with the increasing of the external magnetic field. Rare earth metal can go through a structural phase transition (SPT) at low temperatures, [19] due to the magnetostriction property of KDY $(WO_4)_2$. [16] has reported that applying an external magnetic field that is parallel to the (*a,* or *b*)

crystallographic axes of the material can exhibit an unexpected linearly positive or negative jump in the strain, with the increase of the magnetic field Also, after switching the direction of the magnetic field and going back to the zero field, the material behaves unexpectedly with a no jump in the strain. The material underwent a change in the magnetostriction with applied external field, and that led to a no jump back to the original starting point. Additionally, that led to either a higher or a lower returning point that corresponds to the (*a*, or *b*) axes respectively.

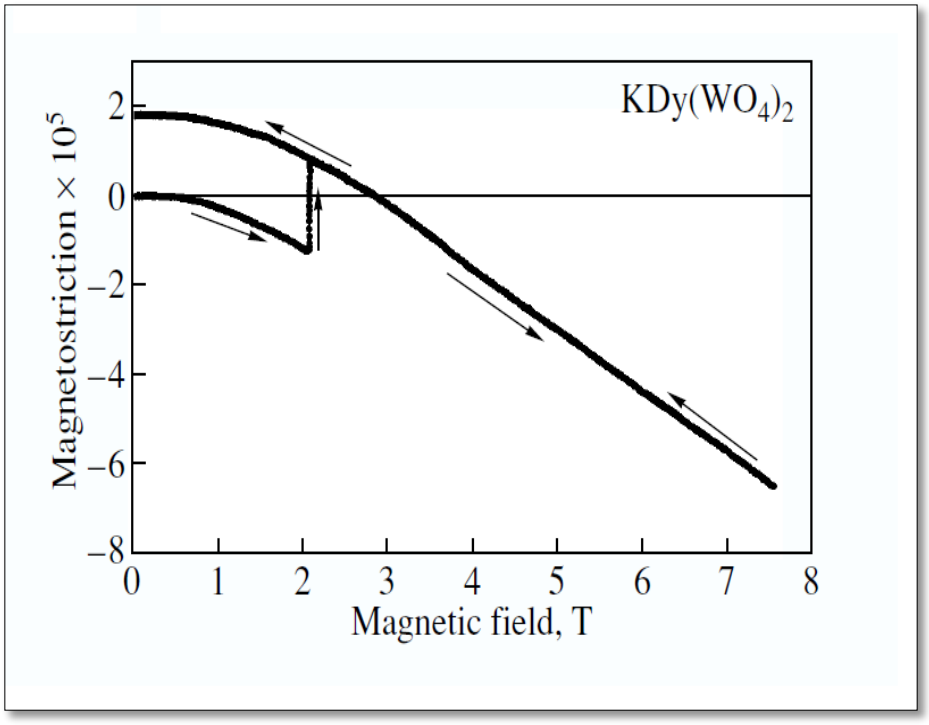

Figure 6. The magnetostriction of $KDy(WO_4)_2$ single crystal [27].

The research group in [27] has reported that the switch remained even after applying another external magnetic field, and the new jump in the strain vanishes only after

heating the sample to a higher temperature above the SPT temperature and then cooling it down to its initial temperature. Such phenomena is being studied by this research and will be applying such techniques to magneto-optical measurement of $KEu(WO_4)_2$.

In another study [28], it's been also shown the magnetostriction measurement on rare earth double tungstate. A potassium rare earth double tungstate $KRe(WO_4)_2$ such as $KDY(WO_4)_2$ were shown to go under a structural phase transition induced by the Jahn-Teller effect or by a strong magnetic field. The experiments in [28] were conducted by inducing a magnetic field parallel to three axes of the material; *a*- , *b*-, and *c*- axes, and in the temperature range from 4.2 to 16.8 K. The results indicated a magnetostriction jump. In addition to that, a hysteretic behavior and an absence of magnetostriction jumps were observed at a temperature of 5.8 K while sweeping the magnetic field along the *b* axes from – 11 T to 11 T and then back to -11 T [28]. This could relate to the tunability of $KRe(WO_4)_2$ under a lower magnetic field, and at low temperatures.

Dr. Borowiec et.al research group [29] has reported the magneto optical effect in rare earth double tungstate. A structural phase transition under a high magnetic field was detected when the Zeeman magneto optical experiment were performed on the single crystal potassium erbium double tungstate [29].

Those reports were experimenting on a single crystal potassium rare earth double tungstate magneto optical effect, and their report was performed under a high magnetic field of up to 5T, and in cryogenic temperatures. In this research, the room temperature magneto optical study will be performed on potassium europium double tungstate, and a magnetic field strength of up to 1.5 T.

3. PRINCIPLES OF MAGNETO-OPTICAL SPECTROSCOPY

This section describes the theory and the principles of the magneto optical Kerr effect (MOKE), and the magnetic circular dichroism (MCD). It is important to mention here that depending on the orientation of the applied magnetic field to the surface of the magnetic sample, one can have three different geometries; polar, longitudinal, and transverse. As shown in Figure 7.

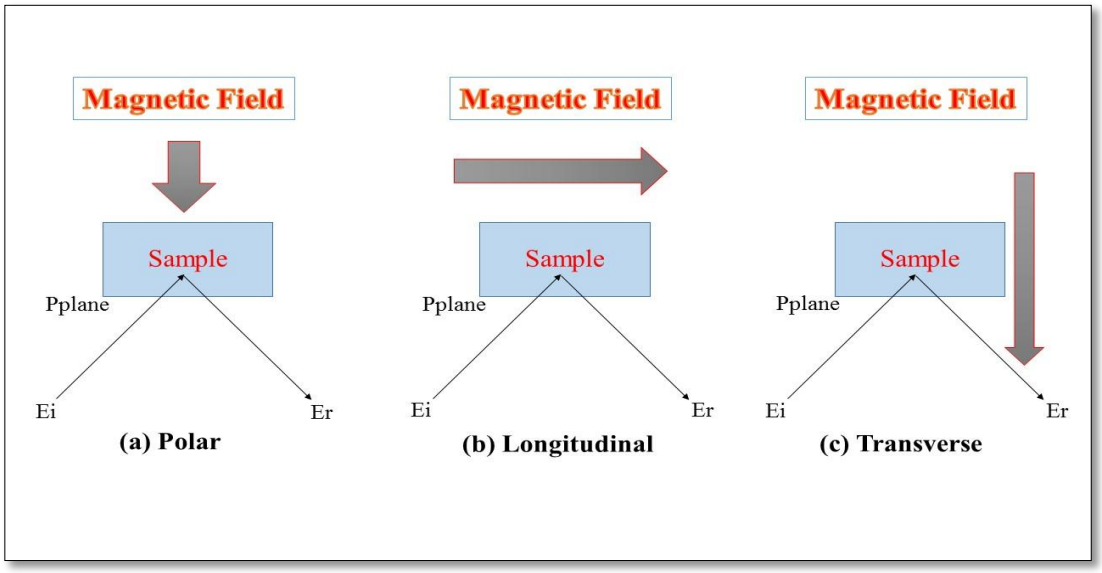

Figure 7. Three geometries of MO. Polar, (b) Longitudinal, and (c) Transverse geometry. ***P****plane plane of incident.* ***E****i: incident electric field.* ***E****r: reflected electric field.*

In the polar geometry, the magnetic field and the linearly polarized light are perpendicular to the surface of the sample; the linearly polarized light is reflected using a mirror that is 45 degrees from the sample [30]. This geometry will be the main orientation for Magneto optical Kerr effect (MOKE) spectroscopy, and the reflection

mode in the Magnetic Circular Dichorism (MCD) spectroscopy. Figure 7A illustrates the polar geometry.

In the Longitudinal geometry, the magnetic field is parallel to the magnetic sample; linearly polarized light is applied to the sample with a specific incident angle, and then reflected. This geometry will be the main geometry for the Magneto optical (MO) for testing the wide band gap materials $KEu(WO_4)_2$, $BaMg_2Al_{16}O_{27}$:Eu,Mn, $(Sr,Mn)_2SiO_4$:Eu. Figure 7B shows the longitudinal geometry.

In the transverse geometry, the magnetic field is perpendicular to magnetic transparent sample. The linearly polarized light propagates through the transparent magnetic sample. Figure 7C shows the transverse geometry.

3-1 Magneto-Optical Kerr Effect (MOKE) Sepctroscopy

In MOKE spectroscopy, a linearly polarized propagated wave is induced on the sample, and reflected by the surface of the sample. Every material has as its own reflection coefficient *r* that depends on the refractive index *N*, and the permittivity ε, is expressed below with the absence of the magnetic field. The coefficient *r* is expressed by the ratio between the reflected and the incident electric field.

$$r = \frac{E^r}{E^i} \tag{3.1}$$

Where $\boldsymbol{E^r}$ is the reflected electric field vector, and $\boldsymbol{E^i}$ is the incident electric field vector.

As a result, a force exerted by the incident electric field vector $\boldsymbol{E}$ induced on the sample is observed and starts to oscillate the electrons with a velocity $\boldsymbol{V}$ in the sample [31], [5].

$$F_E = qE_E \tag{3.2}$$

According to Lorentz force law; applying an external magnetic field will generate new electric field vector $\boldsymbol{E_B}$ that has the same direction as the magnetic force vector $\boldsymbol{F_B}$, and that's due to the interaction between the oscillated electrons with the electron charge q, and the magnetic field vector $\boldsymbol{B}$.

$$F = F_E + F_B = qE + qV \times B = q(E + V \times B) = q(E_E + E_B) \tag{3.3}$$

The new electric field vector $\boldsymbol{E_B}$, also known as the Kerr component K, is perpendicular to the magnetization of the sample $\boldsymbol{M}$, and to the electric field vector $\boldsymbol{E_E}$ [5]. The resulting K vector has an amplitude that depends on the spontaneous magnetization of the material. The resulting reflected waves with the reduced (due to the transmission through the sample) reflected electric field vector $\boldsymbol{E}'$ are merged with the component K, generating two angles to allow the characterization of the polarized elliptically light: the Kerr rotation Θ_k, and the Kerr ellipticity ε_k [32].

Two types of electric fields are usually accommodated with the MOKE spectroscopy, depending on their orientations to the incident plane: *s*-polarized, and *p*-polarized. The *s*-polarized light is perpendicular to the incident plane, whereas the *p*-polarized light is parallel to the incident plane [5]; therefore, the material's reflection coefficients r can be expressed according to two types of the electric fields by

$$r_{ss} = \frac{E_s^r}{E_s^i} \tag{3.4}$$

$$r_{pp} = \frac{E_p^r}{E_p^i} \tag{3.5}$$

Therefore, the reflection coefficients can be exemplified in a matrix form [5]

$$\begin{bmatrix} E_S^r \\ E_P^r \end{bmatrix} = \begin{bmatrix} r_{SS} & 0 \\ 0 & r_{PP} \end{bmatrix} \begin{bmatrix} E_S^i \\ E_P^i \end{bmatrix} = \begin{bmatrix} r_{SS} E_S^i \\ r_{PP} E_P^i \end{bmatrix} \tag{3.6}$$

In which $\boldsymbol{E_S^r}$ is the reflected s-polarized field, and $\boldsymbol{E_P^r}$ is the *p*-polarized field. The small generated $\boldsymbol{K}$ vector plays a role in the reflection coefficients. When the magnetic field is present, the *s*-polarized and the *p*-polarized incident lights generate a $\boldsymbol{K}$ vector in the form of a small *p*-polarized and a small *s*-polarized light respectively. The new reflection coefficients are expressed below by

$$r_{ps} = \frac{E_p^r}{E_s^i} \tag{3.7}$$

$$r_{sp} = \frac{E_s^r}{E_p^i} \tag{3.8}$$

Therefore, the matrix in (3.1.6) becomes

$$\begin{bmatrix} E_S^r \\ E_P^r \end{bmatrix} = \begin{bmatrix} r_{SS} & r_{SP} \\ r_{PS} & r_{PP} \end{bmatrix} \begin{bmatrix} E_S^i \\ E_P^i \end{bmatrix} = \begin{bmatrix} r_{SS} E_S^i & + & r_{SP} E_P^i \\ r_{PS} E_S^i & + & r_{PP} E_P^i \end{bmatrix} \tag{3.9}$$

And so, one can obtain the ratio of r_{ps} to r_{ss}, to Kerr rotation of *s*-polarized light Θ_{ks}, and the Kerr ellipticity of *s*-polarized light ε_{ks}, and the ratio of r_{sp} to r_{pp}, to Kerr rotation of *p*-polarized light Θ_{kp}, and the Kerr ellipticity of p-polarized light ε_{kp} presented by

$$X_{rs} = \frac{r_{PS}}{r_{ss}} \approx \Theta_{KS} + \mathrm{j}\varepsilon_{KS} \tag{3.10}$$

$$X_{rp} = \frac{r_{SP}}{r_{PP}} \approx \Theta_{KP} + \mathrm{j}\varepsilon_{KP} \tag{3.11}$$

Detailed derivations of (3.10), and (3.11) are found in [5].

3-2 Magnetic Circular Dichroism (MCD)

In an assumed to be a diluted magnetic semiconductor (DMS), a large Zeeman splitting in the structural band of the DMS occurs due to the *s, p-d* electrons exchange interaction, which determines the optical and the magnetic properties of a DMS, and that causes polarization dependent optical anisotropies (also known as the magneto optical effect) [15]. Such anisotropic optical absorption causes magnetic circular dichroism (MCD) effect, therefore, MCD is the most powerful tool that detects such interaction.

In MCD spectroscopy, a left-and right-circularly polarized (LCP/RCP) propagated wave is induced on the sample, and reflected by the surface of the sample. LCP differs from RCP by a phase difference of $\pi/2$ [33]. Therefore the circularly polarized induced electric fields are presented by [33]

$$\text{RCP (E +)} = \left(\frac{E^0}{\sqrt{2}}\right)\left[e_x \cos 2\pi v\,(t - n_+\, z/c) - e_y \sin 2\pi v\,(t - \, n_+\, z/c)\right] \tag{3.12}$$

$$\text{LCP (E −)} = \left(\frac{E^0}{\sqrt{2}}\right)\left[e_x \cos 2\pi v\,(t - n_-\, z/c) + e_y \sin 2\pi v\,(t - \, n_-\, z/c)\right] \tag{3.13}$$

Where $\boldsymbol{E^0}$ is the electric field vector amplitude of the polarization. e_x, e_y are the unit vectors in the coordinate directions. The index of refractions are presented by n_+, n_-, for RCP and LCP respectively [38].

After inducing a magnetic field, a Zeeman splitting occurs in the semiconductor band structure due to the *s, p-d* spin polarized exchange interaction. The Zeeman splitting energy $\Delta\boldsymbol{E}$ is explained in the equation below between the valence and the conduction band of the wurtzite semiconductor [34].

$$\Delta\boldsymbol{E} \;=\; (N_0\beta \;-\; N_0\alpha)\mathrm{x}\langle S_z\rangle + \; g^*\mu_B H \tag{3.14}$$

In DMS, the Zeeman splitting is huge due to the strong *s-d* and the *p-d* electron interaction are presented by the $N_0\beta$, and $N_0\alpha$, respectively. The magnetic ions concentration and their average spin due to the magnetic field *H* are presented by the *x*, and S_z, respectively. Whereas g^* is the diamagnetic host semiconductor *g* factor, and Bohr magneton is shown as μ_B [34].

The transmitted light intensity through a DMS sample can be expressed by equation (3.13) under zero magnetic field [15].

$$I = I_0 \exp(-k(E)L) \tag{3.15}$$

Where I_0 is the incident circularly polarized light intensity. At zero magnetic field, $k(E)$ is the optical absorption/reflection coefficient at energy *E*, and *L* is the sample thickness. With the presence of the magnetic field, and with the assumption that the magnetic field will only change the optical absorption spectrum and not the shape of the spectrum, the absorption coefficients for both left (LCP) and right (RCP) circularly polarized light are k^+, and k^-, respectively [15].

$$k^+(E) = k\left(E + \frac{\Delta E}{2}\right) \tag{3.16}$$

$$k^-(E) = k\left(E - \frac{\Delta E}{2}\right) \tag{3.17}$$

MCD spectroscopy detects the Zeeman splitting energy $\Delta \boldsymbol{E}$ from the absorption differences between the left-and right-circularly polarized (LCP/RCP) propagated waves. Therefore, MCD is expressed below.

$$\text{MCD} = -\frac{45}{\pi}\,\Delta E\,\frac{dkL}{dE} \tag{3.18}$$

Where k, L and E are the optical absorption/reflection coefficient, sample thickness, and photon energy, respectively [35], [3]. One can conclude the Zeeman energy splitting can be estimated by the undeviating evaluation of the experimentally measured MCD and dkL/dE spectra.

It is very important to note here that a one degree of MCD signal corresponds to 7% difference of the transmitted/reflected light intensity [15]. Also, the obtained optical absorptions/reflection is caused by the different index of refraction of the two circularly polarized lights, and the difference in the absorption/reflection coefficients causes the dichroism in the obtained MCD signal under the magnetic field [33].

4. METHODOLOGY

This section discusses the analytical and the methodology approach for the MOKE spectroscopy, MCD spectroscopy, and MO technique in the three different geometries. As stated earlier, there are three geometries for every magneto optical experiment: Polar, Longitudinal, and transverse. Those geometries are derived from the direction of the magnetic field with respect to the incident plane and the sample surface.

4-1 Polar Geometry

4-1-1 MOKE Spectroscopy

In the polar MOKE geometry, the magnetic field vector is parallel to the plane of the incidence *Pplane* and normal to the reflecting sample surface. In this setup, the incident linearly polarized light *E* can either be perpendicular to the *Pplane*, which makes it s-polarized, or parallel to the *Pplane*; *p*-polarized. Polar MOKE is the only geometry in which the MOKE signal can be observed at normal incidence [36],[5] because of the comparatively large Kerr rotation Θ_{KS}, and Kerr elllipticity ε_k in small and normal angles of incident [37], which makes it useful for studying the spin polarized transport in semiconductors [30]. Figure 8 illustrates the polar MOKE geometry.

According to [5] equations (3.10), and (3.11) in polar geometry, with complex Kerr rotation and Kerr ellipticity, are shown below

$$X_{rs}^{(polar)} = \frac{r_{ps}^{(Polar)}}{r_{ss}} = \frac{j\mathcal{E}_{\perp}N^{(0)}\cos\varphi^{(0)}}{(N^{(0)}\cos\varphi^{(0)} - N_{z0})(N^{(0)}N_{z0} + \mathcal{E}_0\cos\varphi^{(0)})}$$

$$= \Theta_{KS} + \mathrm{j}\varepsilon_{KS} \qquad (4.1)$$

$$X_{rp}^{(polar)} = \frac{r_{ps}^{(Polar)}}{r_{pp}} = \frac{-j\mathcal{E}_{\perp}N^{(0)}\cos\varphi^{(0)}}{(N^{(0)}\cos\varphi^{(0)} + N_{z0})(N^{(0)}N_{z0} - \mathcal{E}_0\cos\varphi^{(0)})}$$

$$= \Theta_{KP} + j\varepsilon_{KP} \qquad (4.2)$$

In which N_{z0} and $N^{(0)}$ are the complex indices of refraction. In this case, they are for the material and the medium, which is air. Since those equations include the sine and cosine components, it is necessary to observe that at incident angle φ = 0, or 90°, both Kerr rotation and Kerr ellipticity cannot be obtained. Which is due to the incapability of applying the Lorentz force law at 0°, and from the inability of entering light into the sample at 90° [5].

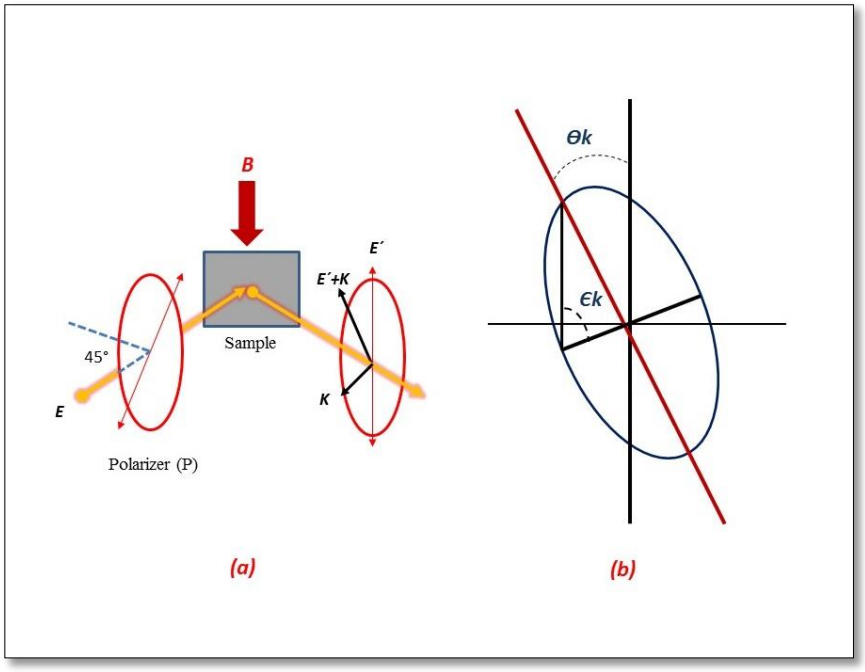

*Figure 8 (a) the polar geometry of the MOKE system, where **E** and **E`** are the incident and the reflected polarized light beam. K is the Kerr vector that was generated from the reflected field under magnetization. Pplane is the incident plane. (b) Shows the Kerr rotation Θ_{KS}, and Kerr elllipticity ε_k.*

4-1-2 MCD Spectroscopy

In the reflection polar MCD geometry, the magnetic field vector is parallel to the plane of the incidence *Pplane,* and normal to the reflecting ferromagnetic sample surface. The obtained dichroism is resulted from difference of intensities between the reflected circularly polarized lights LCP and RCP, which is due to the polarization dependent complex of refraction X on the ferromagnetic sample [38]. The two circularly polarized lights propagate through the medium in different velocities due to traveling through two different mediums, where the refractive index of one is larger than the other, in this case, air and the sample, combine to a linearly polarized light that is rotated with a MCD rotation angle Θ. See Figure 9.

The measured MCD spectrum at the absorption edge depends on the reflected intensities I_L, and I_R for LCP and RCP respectively, with respect to their angle of incident, and reflected Θi, and the orientation of the magnetic field vector $\boldsymbol{B}$, which in this case is perpendicular to the surface of the ferromagnetic sample.

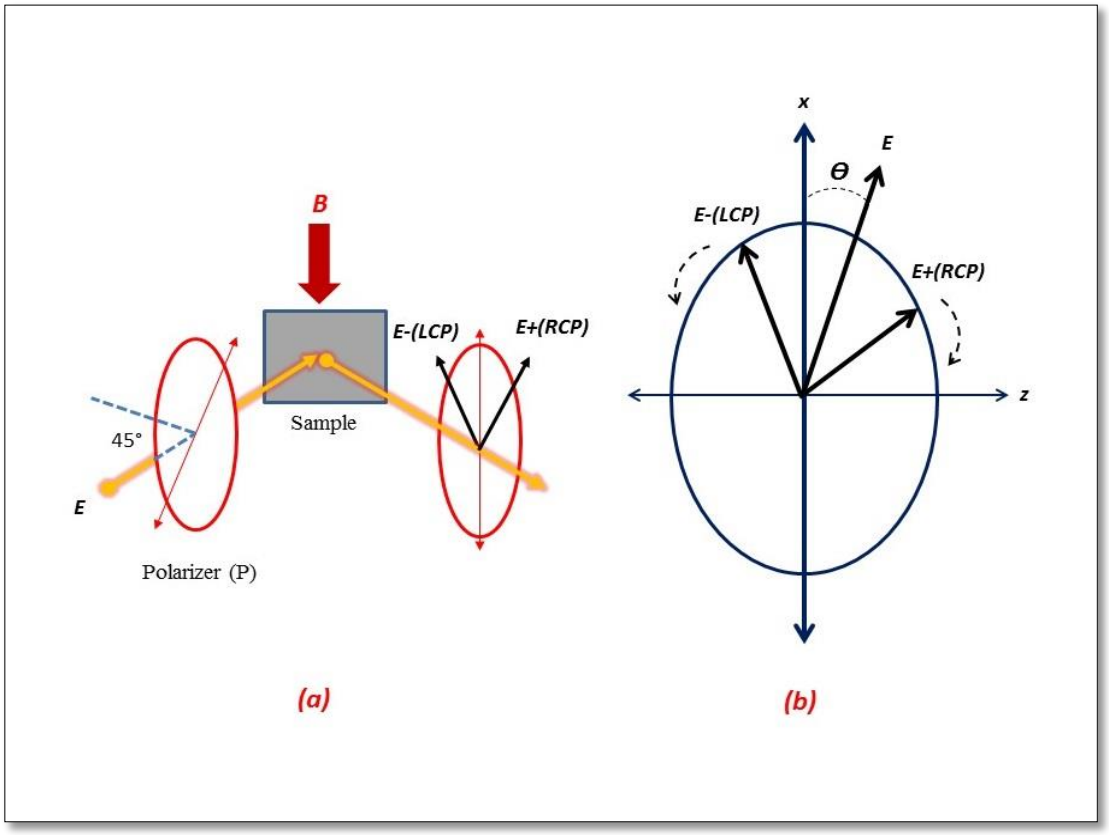

*Figure 9. (a) The polar reflection geometry of the MCD system, where **E** is the incident wave, LCP, and RCP.E-(LCP), and E+(RCP) are the reflected circularly polarized wave. (b) Shows the obtained E lineally polarized wave, generated by the LCP, and RCP.*

Therefore, it is important to observe the reflection coefficients of the dielectric material under magnetization in the geometry, thus, one can calculate the complex refractive index *N* of the material, which is defined below [38]

$$N = n - ik \tag{4.3}$$

Where *n* is the index of refraction and *k* is the absorption coefficient, therefore, one can obtain the complex refraction angle *X* by

$$\sin X = \frac{\sin \theta_i}{N} \tag{4.4}$$

The reflected elliptical LCP and RCP can be expressed into *s*-polarized, and *p*-polarized components, respectively. As shown below:

$$\begin{bmatrix} A_S \\ A_P \end{bmatrix} = \begin{bmatrix} 1 \\ \pm\, i \end{bmatrix} A_0 \tag{4.4}$$

Where A_0 is the real amplitude of the $\pm$ of the RCP and LCP respectively.

As a result, one can obtain the complex reflection coefficients R_P, R_S of the LCP and RCP respectively for different geometries [38]

$$R_P = \frac{N\cos(\theta i) - \cos(X)}{N\,cos(\theta i) + cos(X)} A_P$$

$$- \frac{\epsilon_{xy} cos(90^\circ - \alpha + X)\cos(\theta i)}{Ncos(X)[Ncos(\theta i) + \cos(X)][Ncos(X) + cox(\theta i)]} A_S \tag{4.5}$$

$$R_S = \frac{N\cos(\theta i) - \cos(X)}{N\,cos(\theta i) + cos(X)} A_S$$

$$- \frac{\epsilon_{xy} cos(90^\circ - \alpha - X)\cos(\theta i)}{Ncos(X)[Ncos(\theta i) + \cos(X)][Ncos(X) + cox(\theta i)]} A_P \tag{4.6}$$

Where ϵ_{xy} are the frequency dependent off diagonal elements of the dielectric tensor, and α is the angle between the magnetic field vector $\boldsymbol{B}$, and the ferromagnetic sample [38].

4-2 Longitudinal Geometry

This section discusses the general analytical approach for the longitudinal geometry. This geometry will be used for the Magneto-optical (MO) effect experiment. The MO effect is used to observe the change in photo luminesces intensity under the magnetic field.

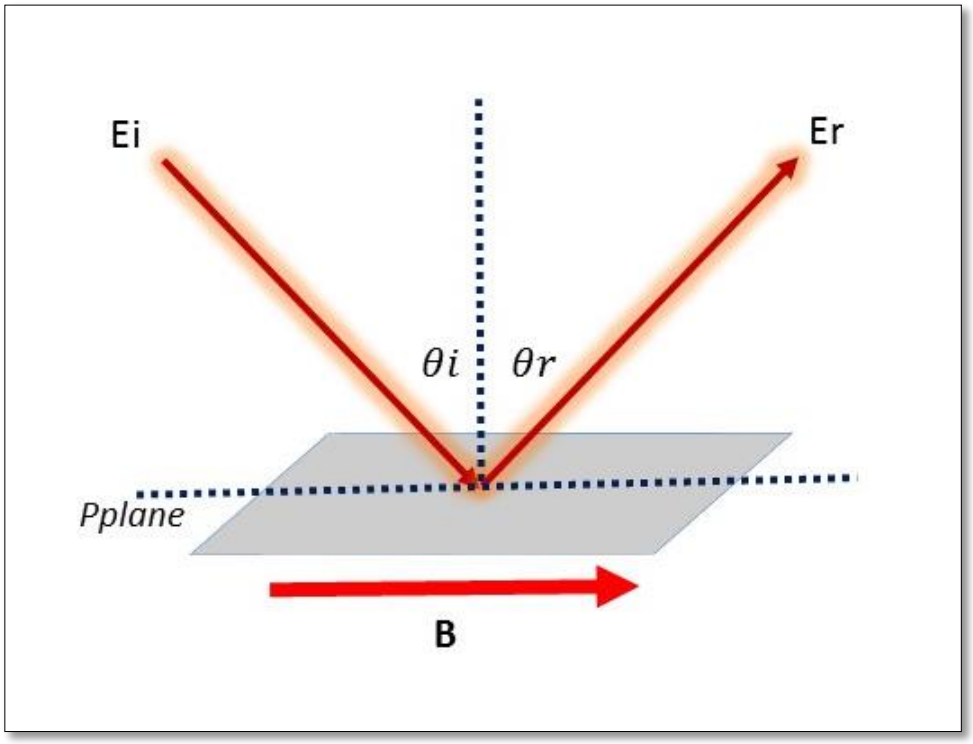

Figure 10. Illustrates the longitudinal geometry for the MO effect experiment, where ***Ei, Er*** *are the incident and reflected waves, respectively.* $\theta i, \theta r$*, are the incident and the reflected angles, respectively.*

In the longitudinal geometry, a polarized propagated wave is induced on the sample, and reflected by the surface of the sample. The magnetic field ***B*** orientation is parallel to both ferromagnetic sample surface and the plane of incident as shown in Figure 10, where the incident angle θi must be equal the reflected angle θr, to avoid any changes in polarization. This geometry will be used as the main configuration for testing the magneto-optical effect of the $KEu(WO_4)_2$.

5. EXPERIMENTAL SETUP

5-1 MOKE Spectroscopy

Development and upgrade of the new MOKE spectrometer was done on the existing MOKE setup. [5]. The MOKE spectroscopy setup was constructed using experimental principles described in [30], [15], [39], and [40]. A polarized and modulated light measurements technique based on the photo-elastic modulator (PEM) technique was used to determine both rotation and ellipticity Kerr parameters simultaneously.

In the typical polar geometry, the light beam must pass through the electromagnet long narrow axial hole, where the sample is mounted between the two magnetic poles [41]. This approach is experimentally challenging because it requires frequent alteration of the optical light probe path using multiple reflecting surfaces. The typical MOKE spectrum is obtained by measuring optical absorption of the sample across a broader spectral range. A mirror-based polar geometry was developed, where the sample and the mirror are placed between the magnetic poles. The incident light and the reflected light will both be reflected by the mirror [30]. The mirror-based polar MOKE idea was taken from [30], one can develop a new sample holder made from nonmagnetic copper, and will be using an Aluminum mirror, which will be positioned 45° from the sample surface. Figure 11 illustrates the new mirror based polar geometry sample holder. For the complete mathematical derivations for using this sample holder, see Appendix A.

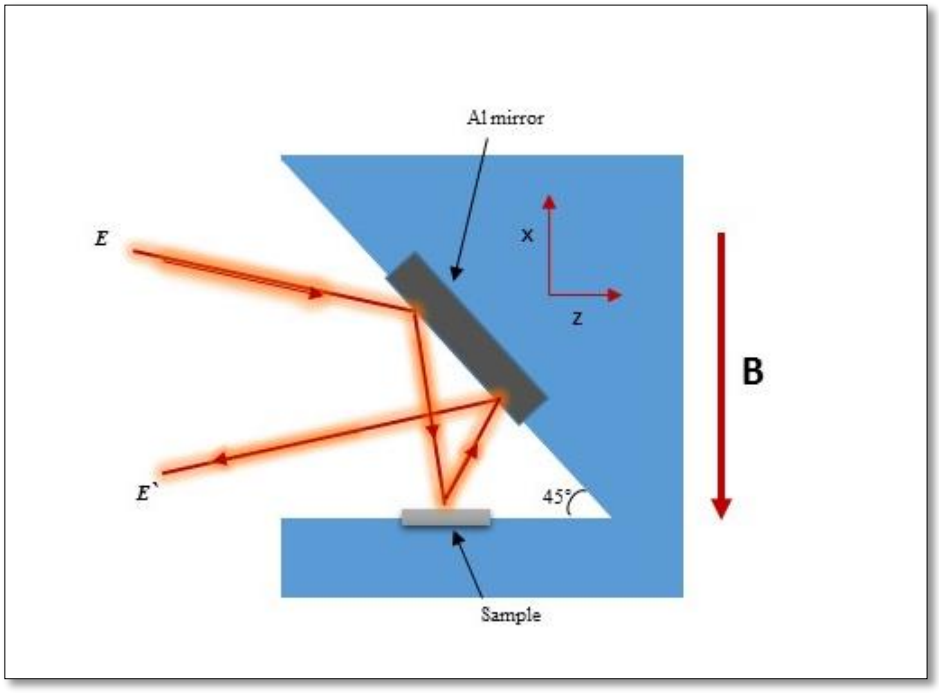

*Figure 11. Illustrates the new mirror-based polar geometry, where **E** and **E`** are the incident and the reflected light beam, and **B** is the magnetic field direction, which is the polar case, is perpendicular to the sample surface.*

At first, a monochromatic light from a broadband Xe-lamp (Spectral Product, model #ASB-XE-175)**)**, and tungsten lamp (Spectral Products, model #ASBN) was dispersed using a monochromator (Spectra Product, model #CM110**)** in the spectral range from 350 nm to 1100 nm and then collimated before being made incident at the first polarizer (Glan-Thompson polarizer**,** model **#**Oriel 13011), where it set at an angle of 45°. Then it gets modulated by the PEM (Hinds Instrument, model #PEM-100**)** at a modulation frequency *f = 100 kHz*. The new sample holder was attached to a cold finger inside of a closed-cycle helium-cryostat (ARS, model #DE-202NI) operating from 8K to 310K in high vacuum condition (1e-7 Torr) between the two electromagnet poles (Lake Shore, Model #EM4-HVA) magnetic poles, where the polarized light ***E*** passes into the cryostat

through a fused silica window in front, is reflected on the sample surface by the Al-mirror, the Al-mirror then captures the reflected light ***E`*** by the sample see Figure 11. After hitting the sample, and after being subjected to a magnetic field up to 1.5 T, the reflected light goes through a second analyzer (Glan-Thompson polarizer, model # Oriel 25011) was used to cross out the polarization. The reflected polarized signal is detected by a silicon-diode detector (DET-200**)**, and then sent to two lock-in-amplifiers (Stanford Research, model# SR830) for both the AC and DC signal. The reference signal for the DC signal of the second lock-in-amplifier is provided by the optical chopper (New Foucs Inc, Model # 3501) operating at ~ 3 kHz, which is placed between the first polarizer and the PEM. Finally, the collected data goes to the computer for analysis. The magnetic field is controlled by the electromagnet, which is powered by the power supply (LakeShore, model # 642), and detected by a Hall probe (LakeShore, HGCT-3020), and controlled by a Gauss meter (LakeShore, 475-DSP). The sample temperature was monitored using a Lake Shore Silicon Diode temperature sensor (Model DT-670B-SD) controlled with Lake Shore 340 temperature controller with a stability of 0.5 K. A LabVIEW PC software was used to remotely control the entire MOKE experiment. Figure 12 describes the MOKE technique in polar geometry.

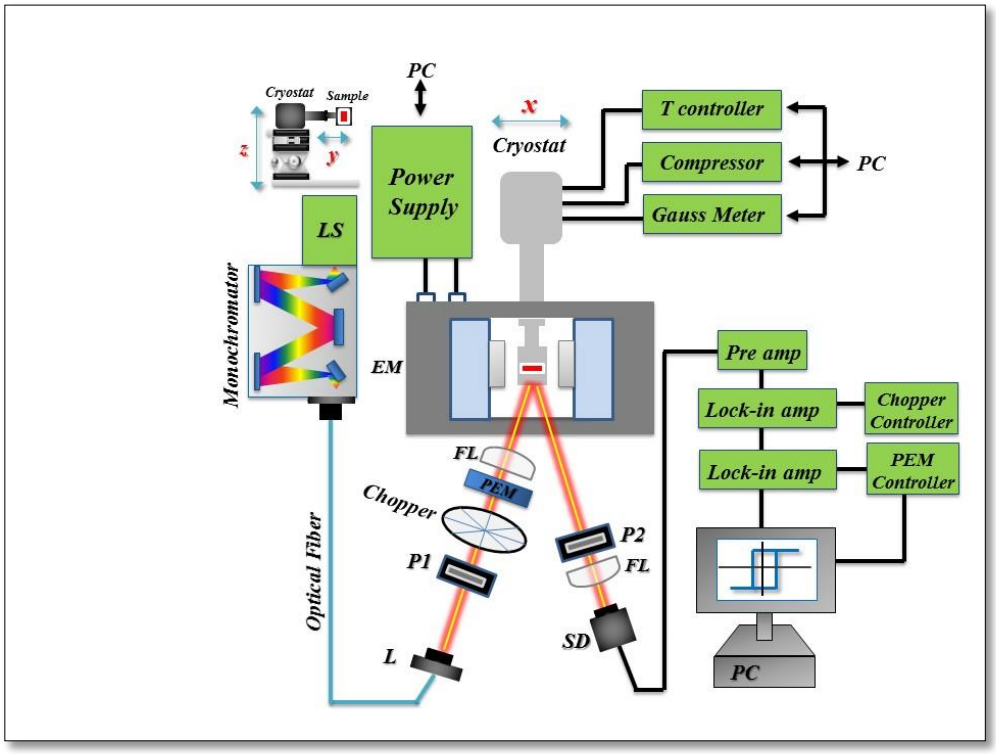

Figure 12. The polar MOKE geometry, mirror based sample holder is used, where LS is the light source, in our case, it is the Xe-lamp. L, P, and P, are the fiber optics coupler collimated lens, the first 45° polarizer, and second polarizer/analyzer, respectively. The signal is detected using the silicon detector (SD). PC is the personal computer where the entire system is remotely controlled. The signal to noise ratio is amplified using the pre amplifier (pre amp).

The MOKE technique measures the rotation of the reflected ellepitivcallt polarized light due to Lorentz force law, whereas MCD measures the difference in absorption. The Physics is completely different, but the experimental setup is close. In the next section, the MCD spectroscopy experimental setup is explained.

5-2 MCD Spectroscopy

The experimental setup of the MCD spectroscopy is similar to the MOKE spectroscopy, in which both are using the same geometry with the same mirror sample holder as described in section 5-2.

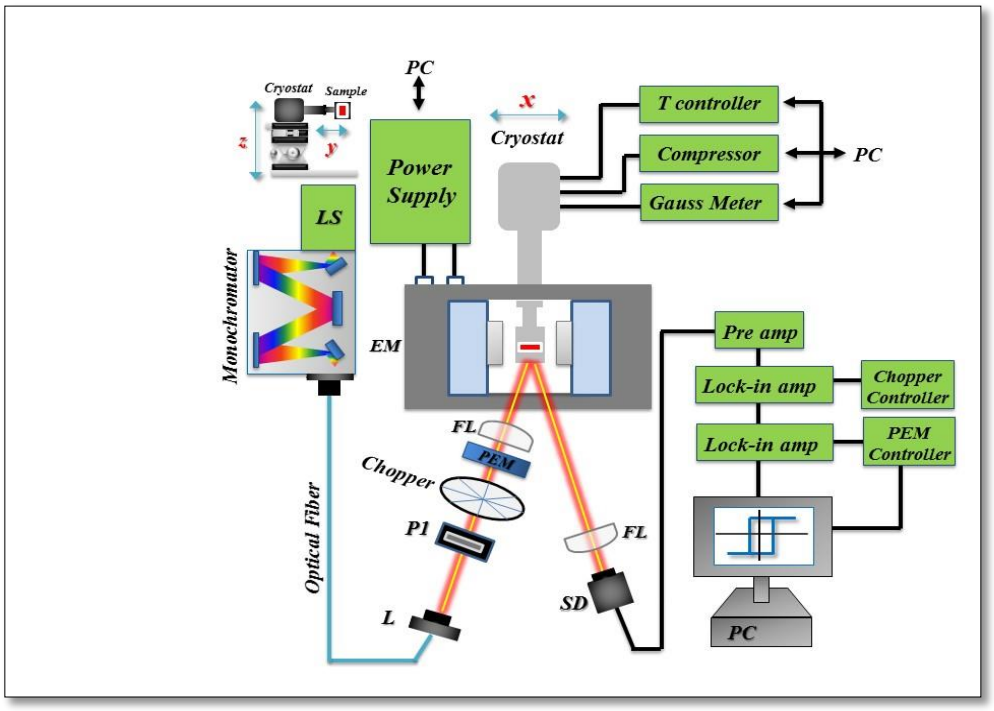

Figure 13. The polar MCD geometry experimental setup, mirror-based sample holder is used, where LS is the light source, in this case, it is the Xe-lamp. L, and P, are the fiber optics coupler collimated lens, and the 45° polarizer, respectively. The signal is detected using the silicon detector (SD). PC is the personal computer where the entire system is remotely controlled. The signal to noise ratio is amplified using the pre amplifier (pre amp).

For the MCD experiment, we have used two light sources, Xe (Xenon) and W (Tungsten) lamps for an operation in combined spectral range between (250-1100) nm. The experimental setup for the MCD spectroscopy differs from the MOKE spectroscopy

by using one polarizer (Glan-Thompson Polarizer, model # Oriel 13011) set at 45°, and a modulation frequency $f = 50\ kHz$. Figure 13 shows the MCD technique in the polar geometry.

5-3 MO Spectroscopy

The Magneto-optical effect can be studied by measuring the photoluminescence (PL) intensity change in when sample is subjected to magnetic field. Due to the limitation of our electromagnet for not being able to magnetize for a longer period of time, the experiment was done using two methods of applied magnetic field; an electromagnet, and a permanent magnet.

The first method includes collecting the temperature and magnetic field dependent spectra, the samples were first mounted on the cold-finger of a closed-cycle helium-cryostat (ARS, model # DE-202NI) operating from 8K to 310K in high vacuum condition(1E-7 Torr) , coupled to an electromagnet (Lake Shore, Model # EM4-HVA). The magnetic field strength was monitored with a Lake Shore Magnet Hall sensor (Lake Shore, Model # HGCT-3020) and a Gaussmeter (Lake Shore, Model 475-DSP). The samples were then excited with a 405-nm Laser Diode with a maximum power of 85 mW. The long-term magnetic field stability was 0.001 T and no magnetic field strength drift was observed during data collection. The sample temperature was monitored using a Lake Shore Silicon Diode temperature sensor (Lake Shore, Model # DT-670B-SD) controlled with Lake Shore 340 temperature controller with a stability of 0.5 K. ThePL signal was detected by using a fiber optic spectrometer (Ocean Optics, Model #

USB2000). The obtained spectra were collected in longitudinal magnetic field geometry. Figure 14, describes the MO spectroscopy experimental setup using an electromagnet.

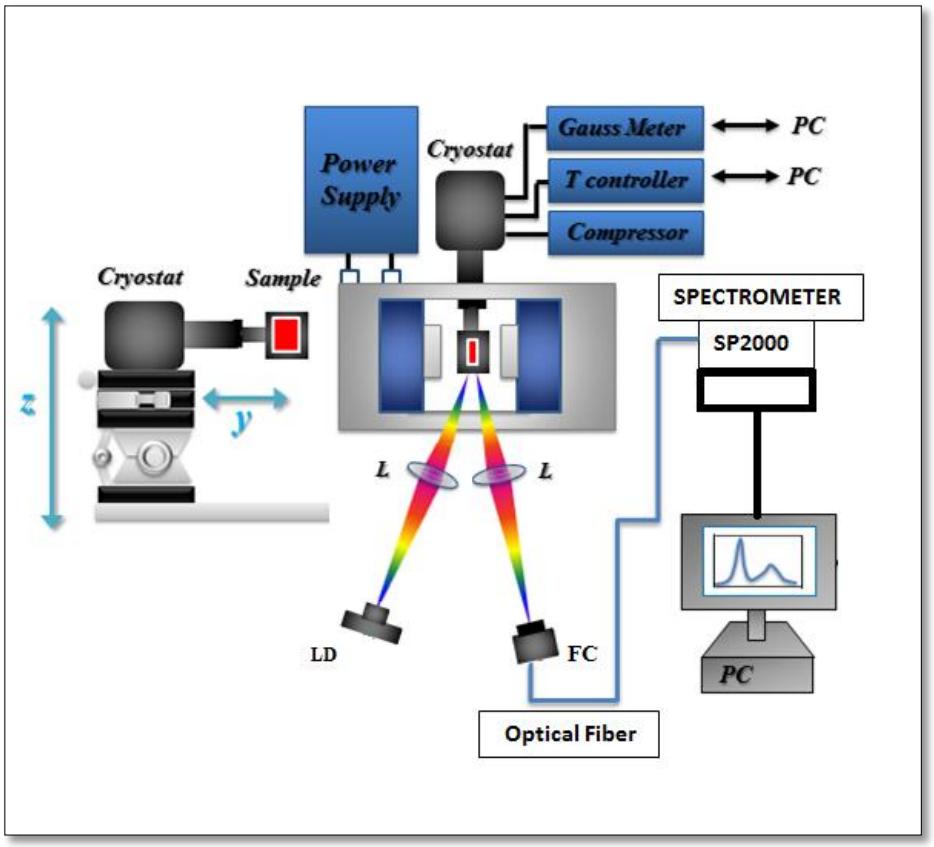

Figure 14. The Longitudinal MO geometry experimental setup, where LD Laser light source. FC is the optical fiber coupler, where the reflected signal is captured.

The electromagnet method was used to obtain the MO effect in temperature controlled settings and less magnetization time. Where the permanent magnet setting took place at room temperature and longer magnetization time. In the second method, the sample was pre-magnetized under a magnetic field strength of 0.94 Tesla for a longer time then the first method was conducted on the sample.

6. GRAPHICAL USER INTERFACE (GUI)

In order to record and plot the MOKE and MCD spectrum and hysteresis loop, one must first develop a graphical user interface (GUI) using LabVIEW code. The code utilizes the different steps of the specific experiment; therefore, one must develop the flow chart in which the code will follow in order to record, store, and plot the obtained data. The LabVIEW code for MOKE and MCD is similar since both techniques involve the same hardware; however, the difference is in the specific experimental setup configuration requirements. The LabVIEW code for the experiment is the same, however, Figure 15 shows the flow chart of the automated data collection process for obtaining the MOKE and the MCD spectra measurement. As for hysteresis loop, the experiment flow chart is the same except that there is no scanning over the spectral range. A detailed description of the operation of the GUI is found in Appendix B.

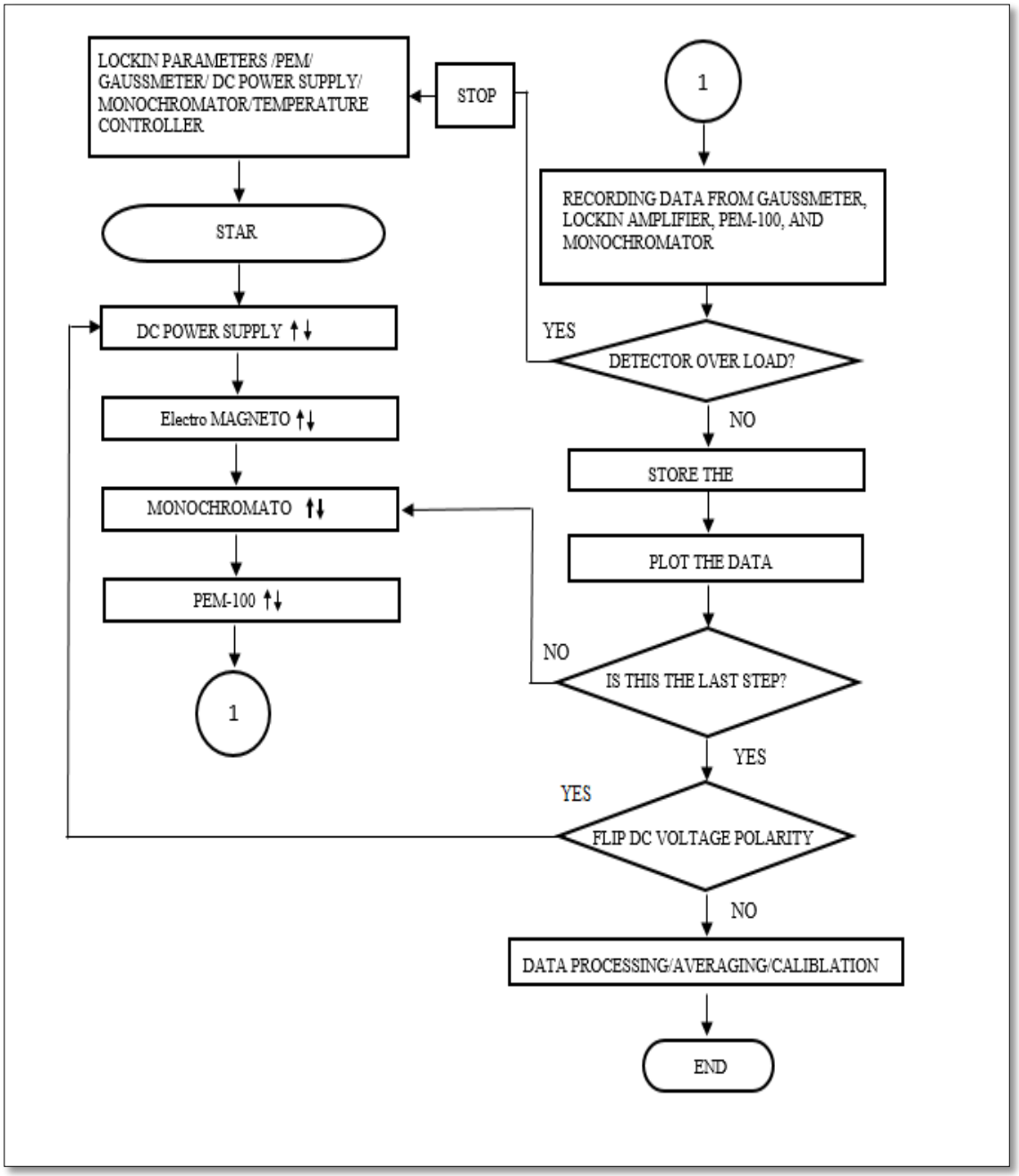

Figure 15. Flow Chart for the Experimental Setup for MOKE and MCD Spectra measurement, controlled by LabVIEW.

7. SAMPLES

We have studied four types of specimens exhibiting magnetic properties.

Test sample #1: amorphous a-AlN:Ni was used to test and optimize the MOKE and the MCD systems. The amorphous a-AlN:Ni sample was supplied by Dr. M. Kordesch in the Department of Physics at Ohio University. The a-AlN thin films were grown by *rf*-sputtering on Si (0001) substrate at low. The films were grown using a 50 mm diameter aluminum target with a few 6 mm diameter pieces of Ni mounted on the target surface [42]. This amorphous AlN:Ni test sample has shown a great magnetic optical isotropy response at room temperature [42], that's why it was chosen for testing our new MOKE and MCD systems.

Test sample # 2 was $Ga_{x-1}\,Mn_x\,As$, with 3% Mn concentration was used as a reference sample to test the MCD system and compare the results with [35]. The sample was synthesized by Drs. K. Ando and H Saito in the National Institute of Advanced Industrial Science and Technology (AIST) in Japan. The thin films sample were grown with (1 1 1) – orientation on sapphire (0 0 0 1) substrates by molecular beam epitaxy (MBE). $Ga_{x-1}\,Mn_x\,As$ thin films were grown at 230° C. In order to avoid any optical interference effects and drag effects during the experiment, the sample thicknesses were chosen to be 50 nm [35]

The research sample # 3 was $Ga_{x-1}\,Mn_x\,As$, which is considered a prototype ferromagnetic diluted magnetic semiconductor (DMS). The research sample $Ga_{1-x}Mn_xAs$ thin films were synthesized by Drs. K. Ando and H Saito in the National Institute of Advanced Industrial Science and Technology (AIST) in Japan. The thin films sample

were grown with (1 1 1) – orientation on InP (0 0 0 1) substrates by molecular beam epitaxy (MBE). Ga_{x-1} Mn_x As thin films were grown at 230° C. In order to avoid any optical interference effects and drag effects during the experiment, the sample thicknesses were chosen to be 50 nm [35]. Different Mn concentration (x) were used to test the strong ferromagnetic response of the thin film. Those Mn concentrations were determined from x-ray photoelectron spectroscopy (XPS), calibrated by electron probe micro-analysis (EPMA), and from a calibrated relation between the amount of Mn beam flux and Mn Knudsen cell temperature, monitored in the growth chamber [35]. The research samples were used to optimize and detect a ferromagnetic response by the MCD technique.

The research sample # 4 was a Potassium Europium Tungstate $KEu(WO_4)_2$. The sample was in a powder form and it was obtained from Phosphor Technology Limited, England, U.K. Samples were prepared in two methods. The first one involved using the powder form where the material was mounted on the sample holder. However, due to the vibration caused by the cryostat due to helium pumping, the powder form failed to work and caused fluctuating in the signal; that's why the second method were used. The second method involved mixing the phosphor powders with a potassium silicate solution (KASIL 2132) and coating the slurry on small BK7 glass substrates. Once dry, the samples were mounted on the longitudinal sample holder and used for analysis. It is important to mention here that both methods showed comparable data with similar results.

8. RESULTS AND DISCUSSION

The main purpose of this project is to develop, upgrade, and test the current MOKE, MCD, and MO spectrometers, and studying different magnetic materials. We have used the a-AlN:Ni samples as test sample for optimizing our MOKE, and MCD systems, for their well-known magnetic properties. The GaMnAs research sample were investigated with different Mn concentration using the MCD spectroscopy. Those samples were tested in the Polar configuration for both MOKE and MCD spectroscopy. A magneto-optical spectrum and hysteresis loops were obtained on those samples. We have also investigated the magneto-optical response/effect of the $KEu(WO_4)_2$ research sample.

8-1 MOKE Results

The results from the MOKE spectrometer consisted of testing the amorphous a-AlN:Ni, test sample for testing and optimizing our system. The results were presented in two ways, first, we obtained the spectrum, then a hysteresis loop is obtained at a specific peak in the spectrum that corresponded to a specific wavelength where the material had responded to under magnetization.

8-1-1 Kerr Rotation of a-AlN:Ni

Figure 16 shows the measured MOKE spectrum in the spectra range from 350 -750 nm using the Xe-lamp. The room temperature MOKE spectrum and MOKE hysteresis was obtained on the amorphous test sample a-AlN:Ni, which was annealed at 900 °C for 5 minutes, and at a maximum applied magnetic field of ± 1.45 [Tesla].

What is seen in Figure 16, and Figure 17 is the Kerr rotation spectra of the *s*-polarized, and *p*-polarized lights, measured as a function of wavelength, and photon energy respectively, in the reflection polar geometry of the amorphous AlN:Ni at room temperature. The obtained MOKE spectra shows prominent characteristics at wavelength value of 550 nm and photon energy of 2.25 eV with a Kerr rotation of 1.05 °. The spectrum shows a negative value on the vertical scale, which is normal due to the physics of the experiment. After the reflected light passes through the analyzer where previous polarization is crossed out, the intensity of the light can either be positive or negative, for positive polarization and negative polarization, respectively. When a positive magnetic field is applied, a positive spin-polarization is obtain, and vice versa. The results in [30] shows a negative value for the Kerr rotation spectrum, which confirms the capability of our system.

Figure 18 shows the MOKE hysteresis loop of the AlN:Ni at 550 nm/ 2.75 eV. The Kerr rotation loops in the polar geometry generated by polarized lights are averaged 20 times, repeating to increase the signal-to-noise ratio. Both Kerr rotations observed by the *s*-polarized, and *p*-polarized lights are symmetrical, in which they both show a clear saturation in the magnetization with increasing of the magnetic field strength $\boldsymbol{B}$ in both direction. It is important to keep in mind that the saturation magnetization of the Kerr rotation polar loop generated is reached at ±0.25 [Tesla].

The obtained Kerr hysteresis loop has an amplitude of 105 [milli-degrees], which matches the amplitude of the MOKE spectra at 550-nm. The amorphous a-AlN:Ni test sample were only tested in the polar MOKE configuration.

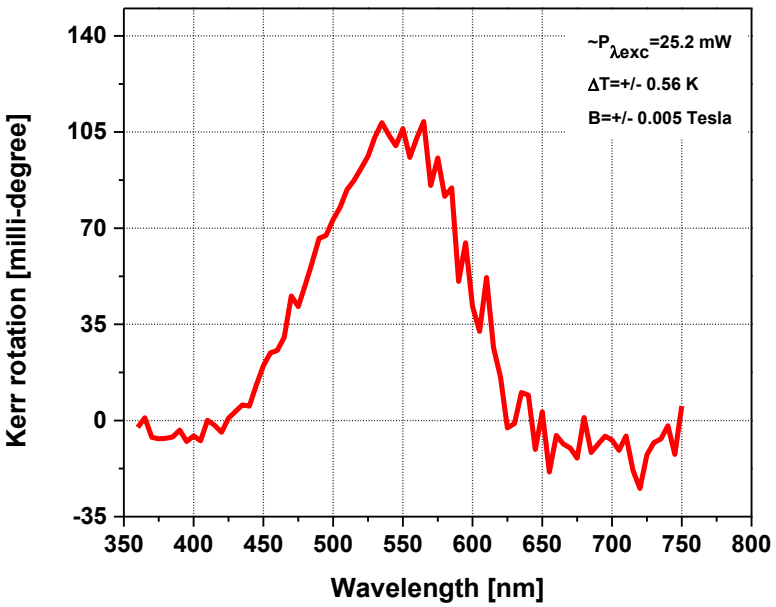

Figure 16. Polar MOKE spectra of a-AlN:Ni at T = 293 K, and B = 1.45 T, as a function of wavelength.

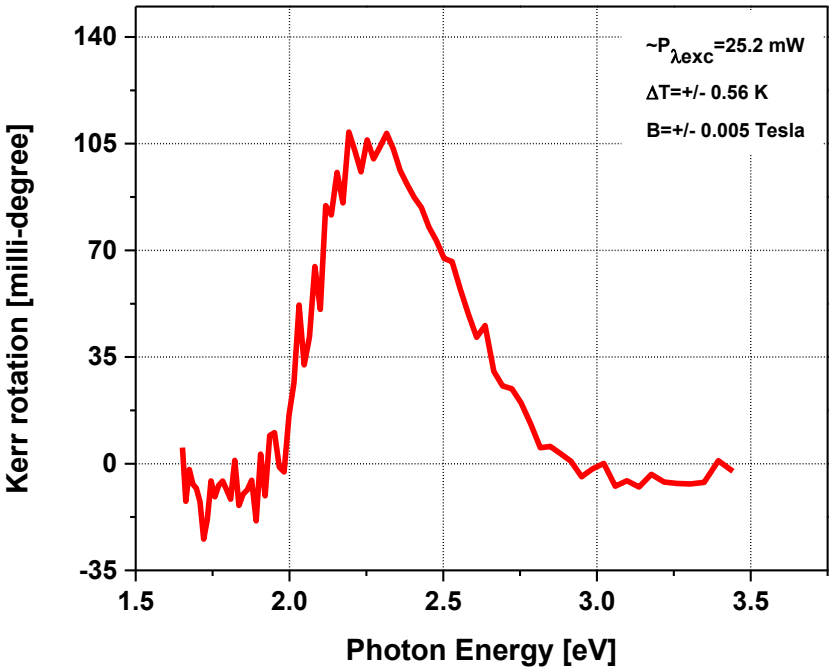

Figure 17. Polar MOKE spectra of a-AlN:Ni at T = 293 K, and B = 1.45 T, as a function of photon Energy.

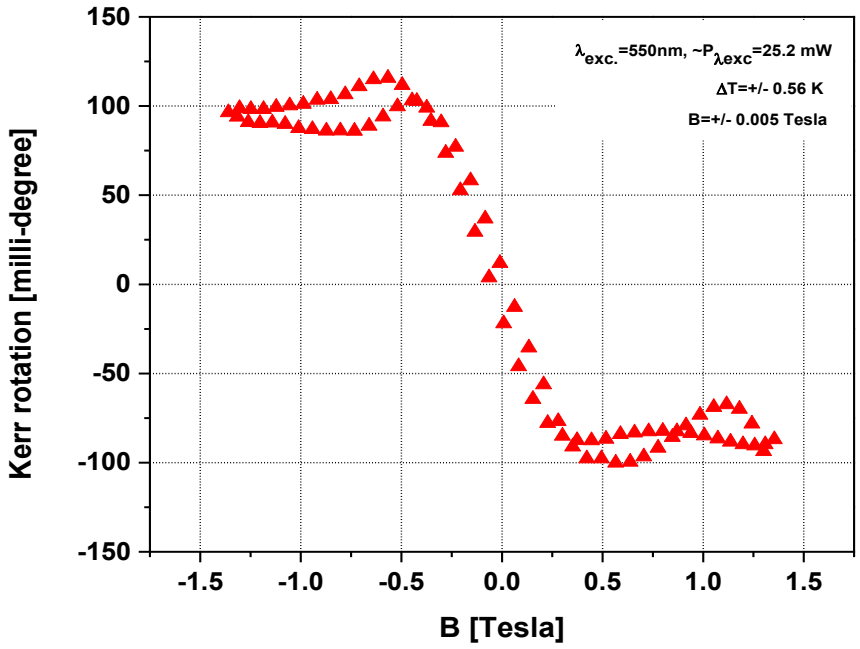

Figure 18. Magnetic field dependence of the Polar MOKE Kerr rotation hysteresis loop for the a-AlN:Ni at 550-nm/ 2.25 eV at T = 293 K, and B = 1.45 T.

The obtained results and the observed symmetry between the measured MOKE spectra and the measured MOKE hysteresis loop confirms the capability of our MOKE system in recording the MOKE spectrum and the MOKE hysteresis loop in the wide range of the magnetic field.

8-2 MCD Results

The results from the MCD spectrometer consist of two parts; the first part was testing the amorphous AlN:Ni test sample for testing and optimizing our system, and for studying the DMS prototype GaMnAs research sample.

8-2-1 MCD Rotation of a-AlN:Ni

The measured MCD spectrum Figure 19 in the spectra range from 350 to 750 nm using the Xe-lamp. The room temperature MCD spectrum and MCD hysteresis were obtained on the amorphous test sample a-AlN:Ni which was annealed at 900 °C for 5 minutes, and at a maximum applied magnetic field of ± 1.6 [Tesla]. We are also able to implement the MCD spectroscopy using the Tungsten lamp (W); this has enabled the system to scan over a broader spectral range (up to 1100 nm).

What is seen in Figure 19 and Figure 20 is the magnetic circular dichroism (MCD) spectra of the left and the right circularly polarized lights, LCP and RCP, respectively. This was measured as a function of wavelength and photon energy respectively, in the reflection polar geometry of the amorphous AlN:Ni at room temperature. The obtained MCD spectra shows prominent characteristics at wavelength value of 550 nm and photon energy of 2.25 eV with a MCD rotation of 0.03165 °.

Figure 21 shows the MCD hysteresis loop of the AlN:Ni at 550 nm/ 2.75 eV. The MCD rotation loops in the polar geometry generated by the LCP and RCP are averaged 20 times, repeating to increase the signal-to-noise ratio. Both MCD rotations observed by the LCP, and RCP are symmetrical and they both show a clear saturation in the magnetization with increasing of the magnetic field strength $\boldsymbol{B}$ in both direction. It is important to keep in mind that the saturation magnetization of the MCD rotation polar loop generated by LCP, and RCP is reached at ±0.5 [Tesla].

The obtained MCD hysteresis loop has an amplitude of 31.65 [milli-degrees], which matches the amplitude of the MCD spectra at 550-nm. The amorphous AlN:Ni test

sample were only tested in the polar MCD configuration. The obtained results and the observed symmetry between the measured MCD spectra and the measured MCD hysteresis loop confirms the capability of the MCD system in recording the MCD spectrum and the MCD hysteresis loop in the wide range of the magnetic field.

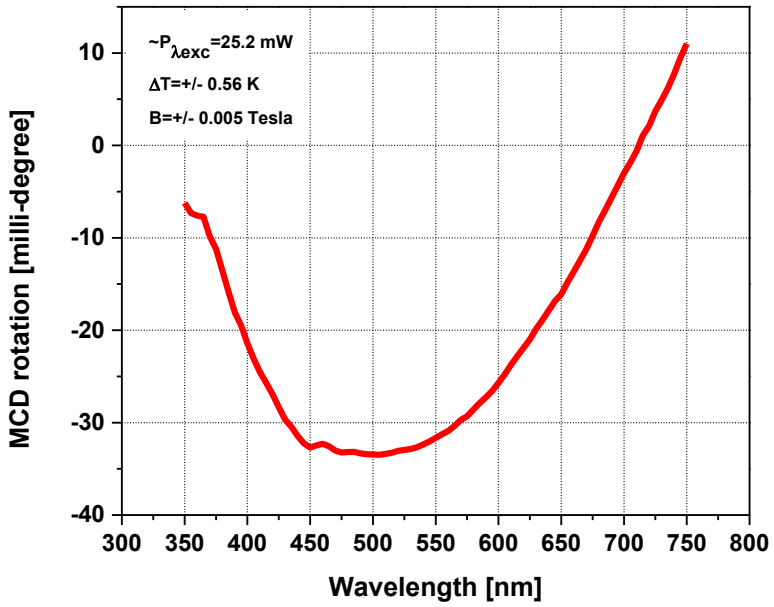

Figure 19. Reflection magnetic circular dichroism (MCD) spectra of amorphous AlN:Ni at T = 293 K, and B = 1.6 T, as a function of wavelength.

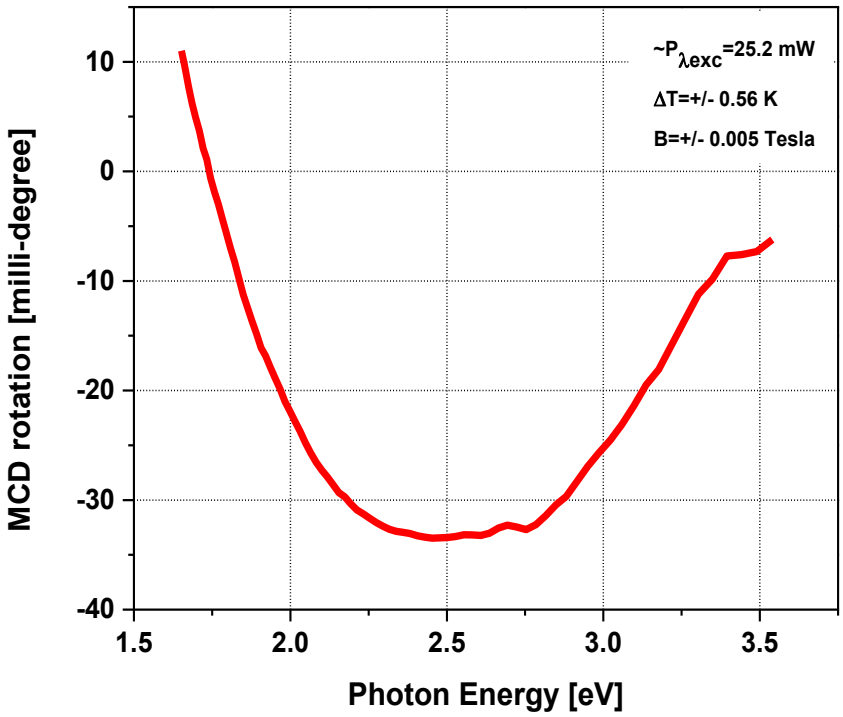

Figure 20. Reflection magnetic circular dichroism (MCD) spectra of amorphous AlN:Ni at T = 293 K, and B = 1.6 T, as a function of photon energy.

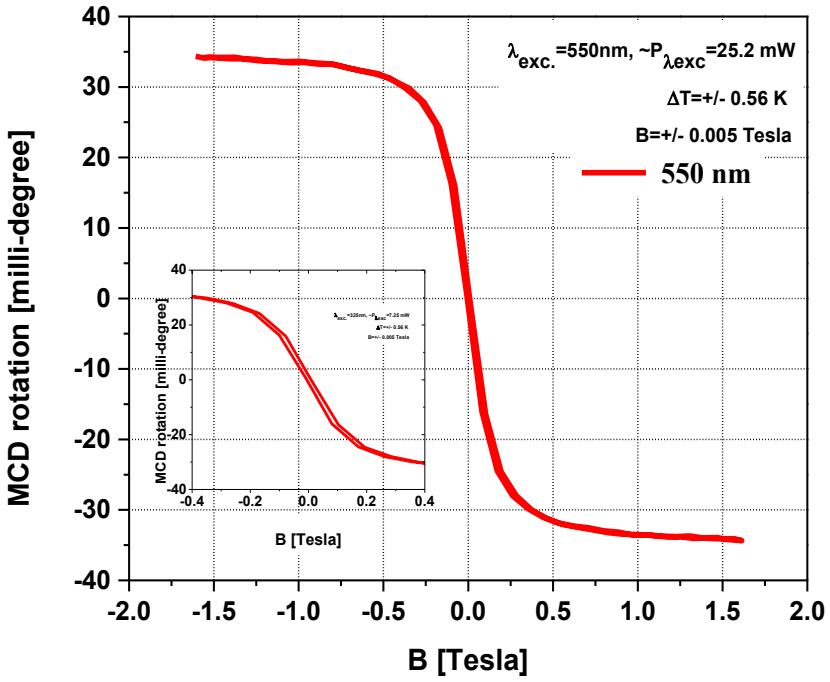

Figure 21. Magnetic field dependence of the Reflection magnetic circular dichroism (MCD) rotation hysteresis loop for the LCD, and RCP at 550-nm/ 2.25 eV of amorphous AlN:Ni at T = 293 K, and B = 1.6 T. Inset shows the magnified memory side of the loop.

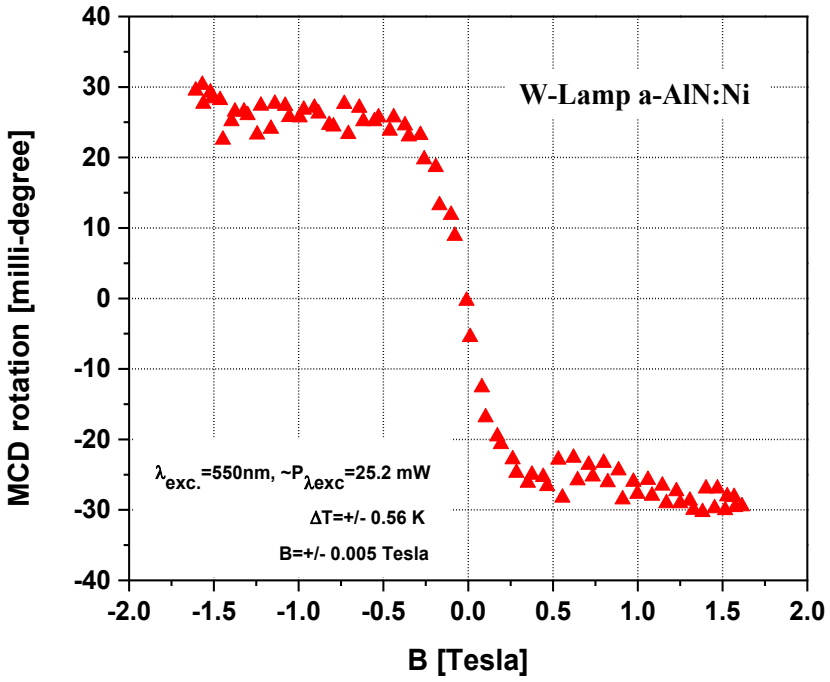

Figure 22. Magnetic field dependence of the Reflection magnetic circular dichroism (MCD) rotation hysteresis loop for the LCD, and RCP at 550-nm/ 2.25 eV of amorphous AlN:Ni using W lamp at T = 293 K, and B = 1.6 T.

As a result, our new MCD system is ready to test the research sample GaMnAs. The results and the analysis of the recorded MCD rotation and MCD hysteresis loop are provided in the following section

8-2-2 MCD Rotation of $Ga_{x-1}\,Mn_x\,As$

For optimizing the new MCD spectroscopy system, the GaMnAs on a sapphire substrate was used. The results obtained from the sample show comparable results obtained from [35] with lower amplitude. The MCD spectrum obtained from [35] shows an amplitude of 100 [milli-degrees], whereas the amplitude of the signal from our new

system shows an amplitude of 20 [milli-degrees]. This difference in intensity is due to having extra optical paths. The new MCD system used an extra mirror and utilizes the reflection mode, whereas the system in [35] uses the transmission mode with no mirrors. The use of extra mirrors and reflection geometry were the reason why our system showed a lower intensity. It is also important to keep in mind, that the same sample was used in both systems. This concludes that the new developed MCD system is ready and can produce similar results of the other MCD systems. Figures below show the MCD spectrum and MCD hysteresis loop on the GaMnAs/Sapphire with 3% Mn concentration.

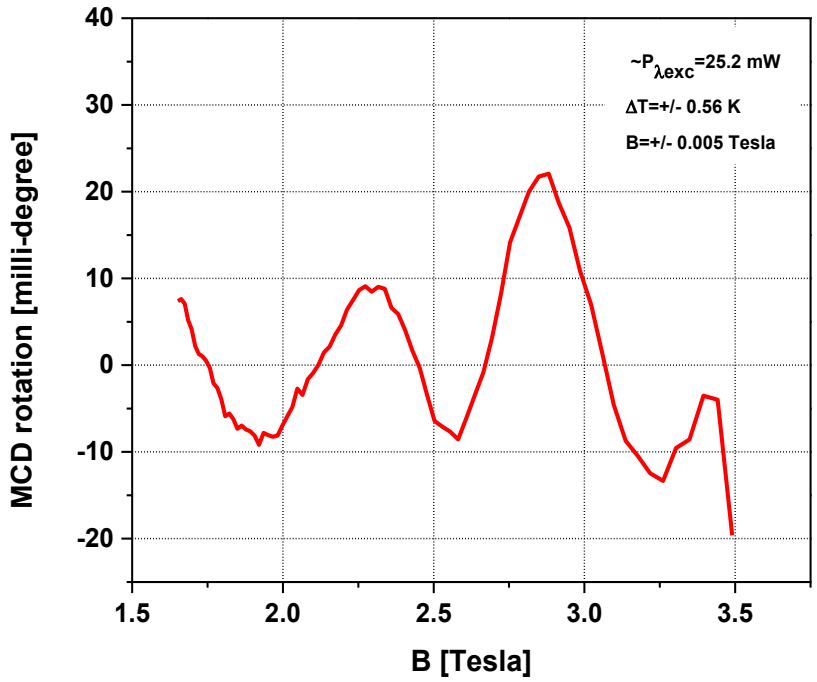

Figure 23 shows the reflection magnetic circular dichroism (MCD) spectra of Ga_{x-1} Mn_x As/sapphire with different 3% Mn concentration at T = 8 K and B = 1 Tesla as a function of photon energy.

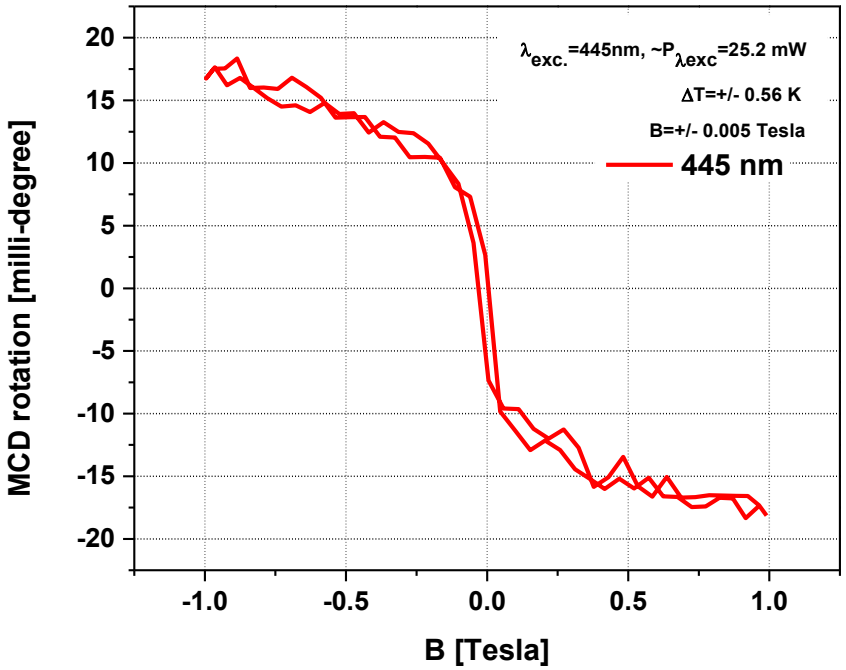

Figure 24 shows the Magnetic field dependence of the GaMnAs/Sapphire with 3% Mn concentration at T = 8 K and B = 1 Tesla.

Figure 25 (a)-(h) show the magnetic circular dichroism (MCD) spectra in the reflection mode for the spectra range from 350 to 750 nm, on the research sample Ga_{x-1} Mn_x As with different Mn concentration as a function of photon energy, measured at T = 8 K and a magnetic field strength ***B*** of up to ±1.0 [Tesla].

The measured MCD spectra shows a projecting positive and negative broad peaks features over the range of photon energies between 1.65 - 3.54 eV as shown in figure 25 (a)-(h). The measured MCD spectrums shows a strong ferromagnetic response from the

$Ga_{x-1}Mn_xAs$ (x = 0.03) as seen in figure 25 (h), which has the highest Mn concentration, where lower Mn concentration such as: x = 0.01 show a paramagnetic respond as seen in Figure 25(b). Spectra (a) shows the MCD spectra of the paramagnetic GaAs. The $Ga_{x-1}Mn_xAs$ in Figure 25 (h, g) show a ferromagnetic respond around photon energies 2.78 eV, and 3.44 eV. That is due to the Zeeman splitting in the energy band due to the s-p-d electron interaction between the semiconductor host material and the magnetic ions. Magnetic field dependency as shown in figure 26, of the $Ga_{x-1}Mn_xAs$ at 3% Mn concentration in the reflection polar geometry at 445-nm and 360-nm.

Figure 26 shows the ferromagnetic MCD hysteresis loop at 445nm from Gax-1 Mnx As (x = 0.03). In addition to that, interestingly, one also observed the ferromagnetic MCD hysteresis loop at 445 nm from $Ga_{x-1}Mn_xAs$ (x = 0.01). However, [35] shows the ferromagnetic hysteresis loop only from x = 0.03 not 0.01. This may be due to the quality of the crystal structure in $Ga_{x-1}Mn_xAs$. $Ga_{x-1}Mn_xAs$ on Sapphire substrate has a lattice mismatch since $Ga_{x-1}Mn_xAs$ is cubic crystal structure and Sapphire is hexagonal structure. On the other hand, InP is cubic structure, $Ga_{x-1}Mn_xAs$ on InP has much less lattice mismatch. Therefore, magnetic anisotropy is better in $Ga_{x-1}Mn_xAs$ on InP. Consequently, this may be the reason why a ferromagnetic hysteresis loop was observed GaAs:Mn (x = 0.01).

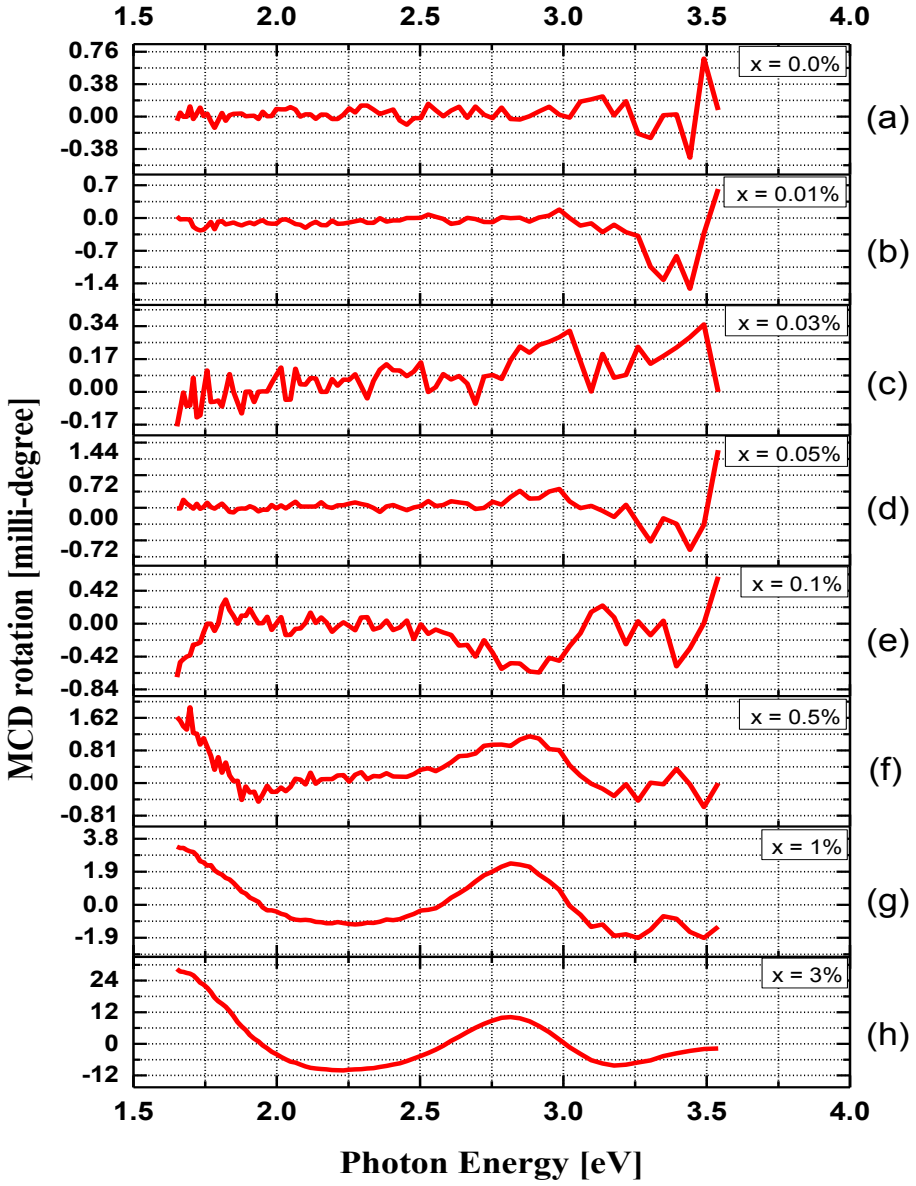

Figure 25. (a)-(h) *Reflection magnetic circular dichroism (MCD) spectra of* $Ga_{x-1}\,Mn_x\,As$ *with different Mn concentration at T = 8 K and B = 1 Tesla as a function of photon energy.*

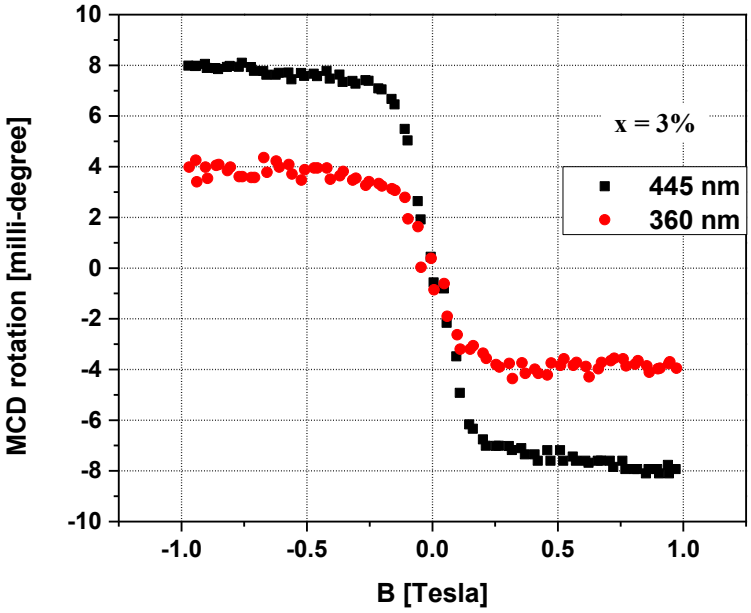

Figure 26. The Magnetic field dependence of the $Ga_{x-1}\,Mn_x\,As$ with Mn concentration of 3% at T = 8 K and B = 1 Tesla.

It is critical to mentioned that the band gap of $Ga_{x-1}\,Mn_x\,As$ is 1.52 [eV], and looking at the spectrum below, one can see two peaks - one peak is around the Gamma critical point (Γ (E_0 and $E_0 + \Delta_0$)) which is 1.52 [eV] and 1.82 [eV] respectively. The other peak around the L-critical point (L (E_1 and $E_1 + \Delta_1$)) is 3.04 [eV], and 3.26 [eV], respectively, [35].

From those peaks, one can only focus on the L-critical point. The reason why that is in the spectrums around the Γ-critical point is because there are multiple optical transitions caused by the impurity background due to Mn ions doping. As a result, the MCD signal becomes very broad and becomes difficult to analyze. On the other hand, L-critical point is less affected by the impurity background and it is easier to analyze [3].

As could be seen from the results below, as the concentration of Mn ions increases, the MCD signal increases as well. The ref. [35], the MCD peaks shifted to a lower energy side whereas the results we obtained did not show any noticeable energy shift to the lower energy side. In [35], transmission MCD setup was used to obtain the MCD signal, whereas the reflection polar MCD setup was used in this project. In addition, the substrate that was used in [35] was sapphire (hexagonal structure), whereas in this project, the substrate was InP (cubic structure). So, these facts may be different from the results we obtained from their results but deeper analysis of these results are still under investigation.

8-3 Magneto-Optical Effect in Phosphors

The existence of the magnetic field dependency in rare earth compounds can have an impact on the intensity of the emission lines of the Potassium Europium Tungstate $KEu(WO_4)_2$; (aka red phosphors). This impact is presented by a linear increase in the intensity of the light with the increase of the magnetic field. Also, due to the magnetostriction property of rare earth ions, the material undergoes a structural phase transition when magnetized. That causes an irreversible transformation in the elastic strain of the rare earth ions. The transformation can be spotted with the magneto-optical measurement as the emission lines produced by rare earth Eu^{3+} is considered the probe in this measurement. Figure 27 below shows the PL spectra obtained from the material with the excitation spectra.

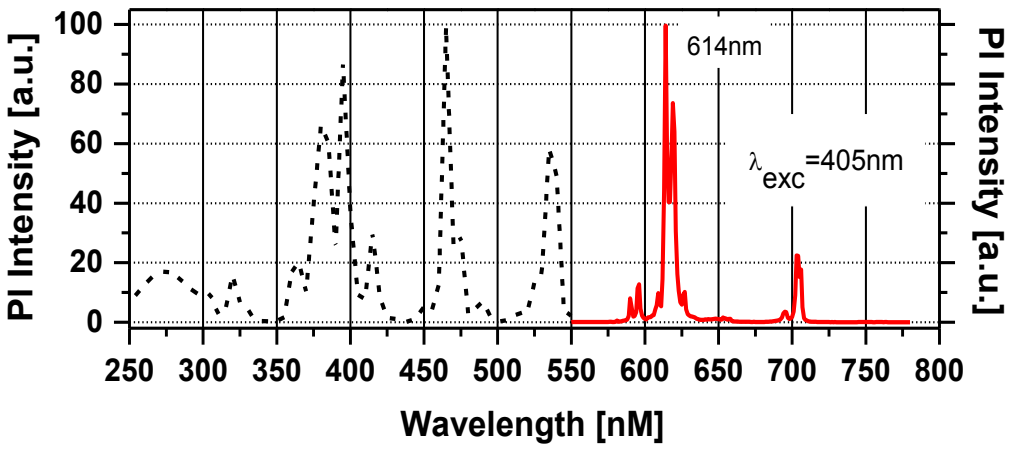

Figure 27. Shows the Room temperature photoluminescence excitation spectra of $KEu(WO_4)_2$ red (R) phosphor monitored at 615 nm. Emission spectra for the phosphor is shown on the right-hand-side of figure. The emission spectra was taken with 405 nm laser excitation.

Indeed, the structural phase transition, and the magneto-optical effect are related to interaction between the rare earth ions with the external field and for the co-operative Jahn-Teller effect in rare earth ions, as the applied magnetic field re-orients the magnetic ions in the material which could lead to a structural phase transition. That causes an increase in the photo luminesce intensity. In this section, several experiments with different variables were conducted on fresh samples of $KEu(WO_4)_2$. This has demonstrated the magnetic field dependency of the Potassium Europium Double Tungstate $KEu(WO_4)_2$.

Figure 28 shows the MO effect of KEu(WO4)2, as a function of intensity. The sample has an emission wavelength peak spectra of 614 nm, when excited with a 405 nm laser diode light source. The obtained spectra showed an electric dipole emission around

614 nm, and a magnetic dipole emission around 569 nm. It can be seen from Figure 28, that the intensity of the light emitted from the sample depends proportionally on the magnetic field strength ***B***. As the magnetic field increases, the intensity of the light increases as well. The data in Figure 28 was collected in a five minutes magnetization interval, meaning, at every ***B*** value, the sample was magnetized for a duration of five minutes. At every interval, the data was collected before, during, and after five minutes of magnetization. It's important to mention here that the intensity of the light remained the same in the before and after magnetization period. The MO effect was observed only during the magnetization, till a sudden jump in the intensity of the light was observed when the magnetic field strength reached 0.7 [Tesla]. The intensity of the light increased dramatically during and after the magnetization. The intensity remained high even after switching off the magnetic field. This sudden increase flagged a point of interest in this material, as the material had exhibited a controllable on/off switching effect when magnetized. The jump in intensity exhibited a locking effect, where the material held its high intensity for a long period of time and failed to show any MO effect after it had relaxed back to its original value.

Figure 29 shows the MO effect of the $KEu(WO_4)_2$ under magnetization in the five minutes magnetization interval, where the sudden linear increase in intensity was shown at the critical field B = 0.7 [Tesla].

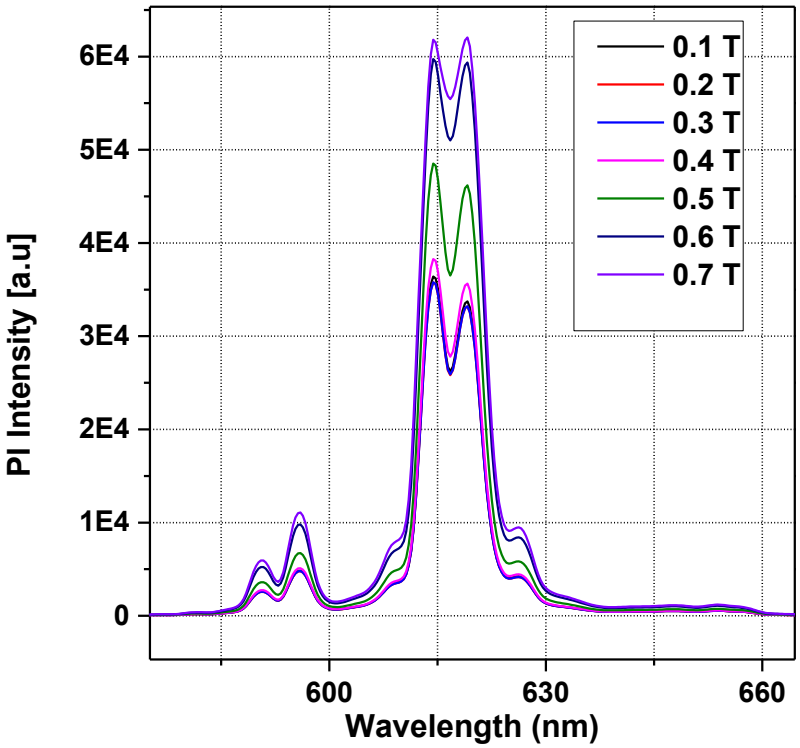

*Figure 28. Illustrates the longitudinal MO effect on $KEu(WO_4)_2$, measured at T = 293 K with increasing **B** from 0.1 – 0.7 [Tesla].*

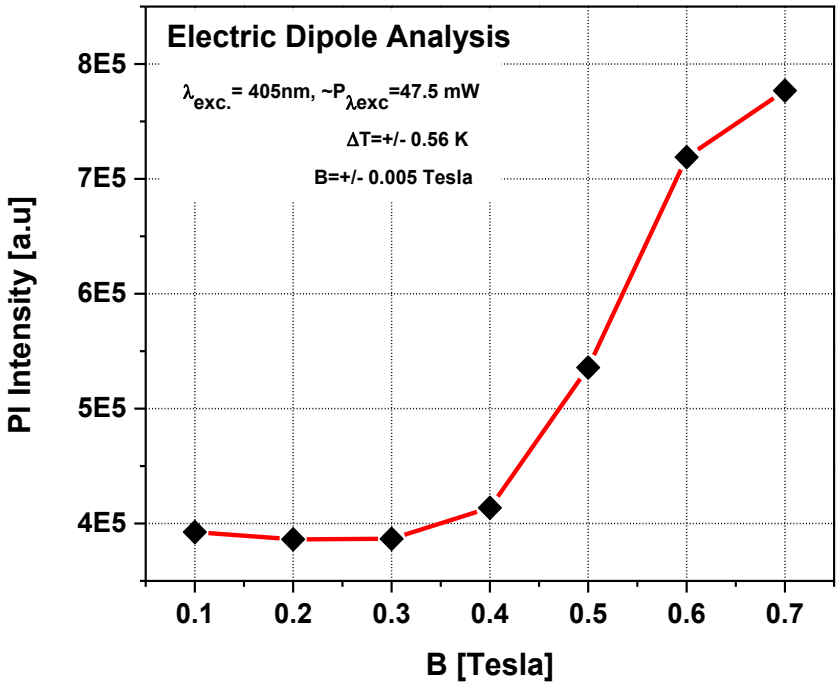

Figure 29. Shows the longitudinal MO effect on $KEu(WO_4)_2$,as a function of magnetic field **B**, measured at T = 293 K, and in the five minutes magnetization interval. Electric dipole analysis.

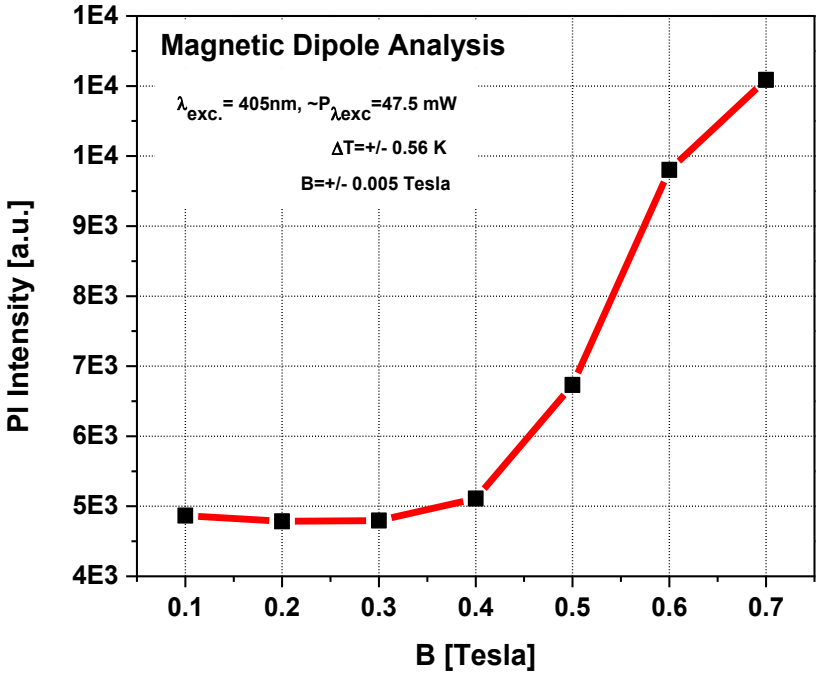

*Figure 30. Shows the longitudinal MO effect on $KEu(WO_4)_2$,as a function of magnetic field **B**, measured at T = 293 K, and in the five minutes magnetization interval. Magnetic dipole analysis.*

As seen from above, both magnetic and electric dipole emissions show the same effect. Due to the linear increase in the intensity of the light, and to understand the nature of the effect, further investigation was conducted on new set of fresh samples. As stated previously the sample failed to show any MO effect after it had relaxed back to its original intensity, therefore, new fresh samples were used at every conducted experiment. To further understand the scope of the effect, one can conduct the experiment on fresh sample with one variable at a time. In the following details, magnetic field ramping rate, magnetic field strength, magnetization time, magnetic field direction, and pre-magnetization variables have been conducted on fresh samples of $KEu(WO_4)_2$.

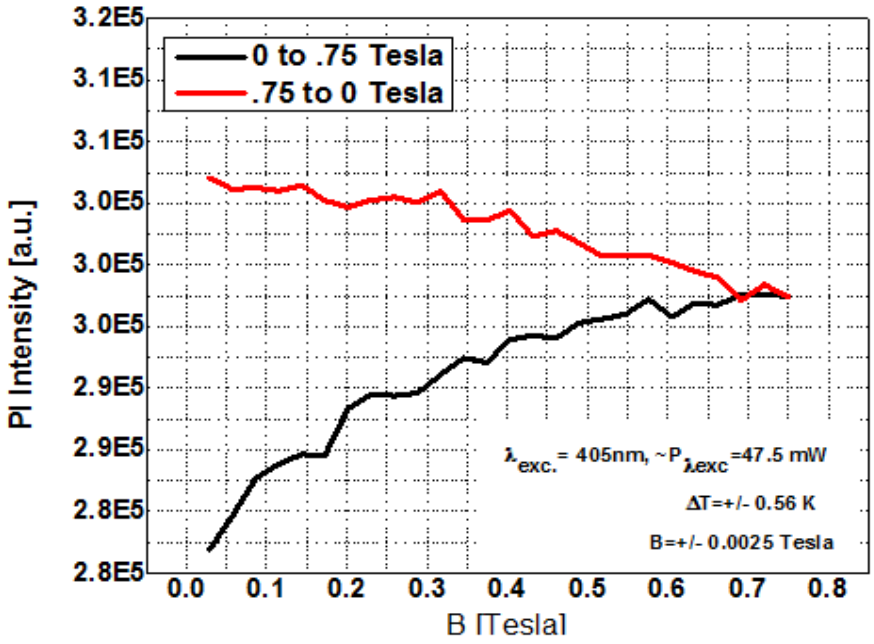

*Figure 31. Illustrates the longitudinal MO effect on $KEu(WO_4)_2$,as a function of magnetic field **B**, at a ramp rate of 2.5 [mTesla/sec], measured at T = 293 K.*

Figure 31 shows the MO effect of the $KEu(WO_4)_2$ as a function of magnetic field ramping rate. The data was collected continuously and without magnetization interval. In this experiment, we have magnetized the sample for a total time of 5 minutes going in one direction of magnetic field (±0.75 [Tesla]) at a ramping rate of 2.5 [mTesla/sec], then we decreased the magnetic field in the same ramp rate back to zero field . As shown in figure 31, the sample exhibit a linear increase in intensity till reaching a magnetic field of 0.7 [Tesla]. The effect had increased and remained higher than it was before magnetization even going back to zero field. The final recorded intensity after going back to zero field, remained higher than the initial one.

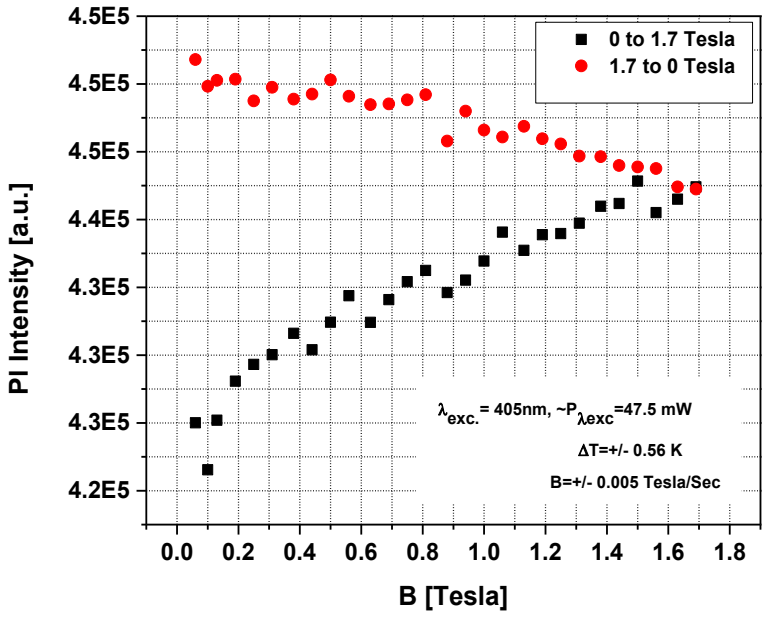

*Figure 32. Illustrates the longitudinal MO effect on $KEu(WO_4)_2$,as a function of magnetic field **B**, at a ramp rate of 5.0 [mTesla/sec], measured at T = 293 K.*

Figure 32 shows the MO effect of a new sample of $KEu(WO_4)_2$, where the ramping rate has been increased to 5.0 [mTesla/sec] for a total magnetization of 2.5 minutes for one magnetic field directions, then the magnetic field was decreased in the same ramp rate back to zero field. The final recorded intensity after going back to zero field, remained higher than the initial one.

This have concluded that magnetization ramping rate dependency doesn't have a strong noticeable effect on the general MO effect of the material. Therefore; the following experimental results were conducted using a 5.0 [mTesla/sec] ramping rate.

As seen from the above results, after reaching the maximum magnetic field, the effect started to saturate, even after turning off the magnetic field.

A Magnetization time dependent experiment was conducted on a fresh sample to demonstrate that the MO effect of the material increases linearly with increasing magnetization time.

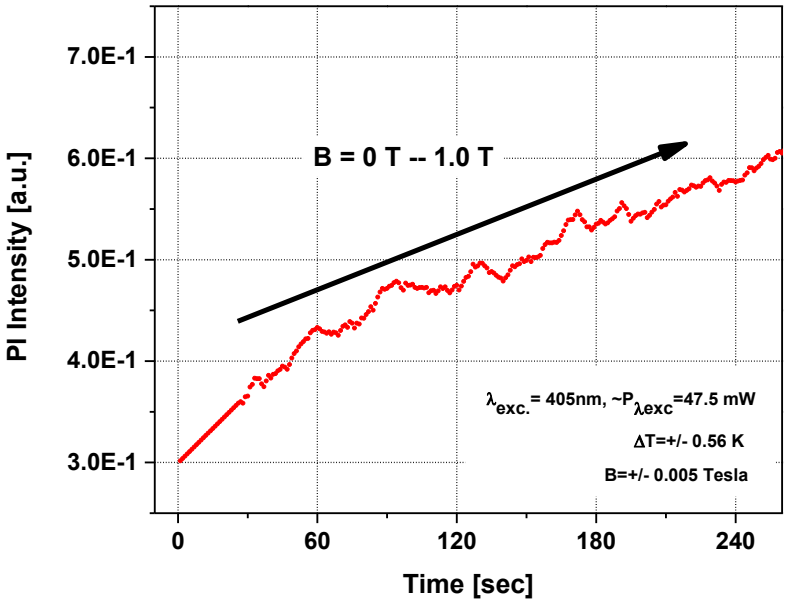

Figure 33. Illustrates the longitudinal MO effect on $KEu(WO_4)_2$,as a function of magnetization time, at a ramp rate of 5.0 [mTesla/sec], measured at T = 293 K..

As seen in figure 33, which shows the magnetization time dependent MO effect on a fresh new sample. In this case, the sample started the magnetization process at a ramping rate of 5.0 [mTesla/sec], tit had reached a total field ***B*** = 1.0 [Tesla] in 260 seconds, in

another experiment, the magnetic field ***B*** was held at 1.0 [Tesla] for 5 minutes, as shown in figure 34.

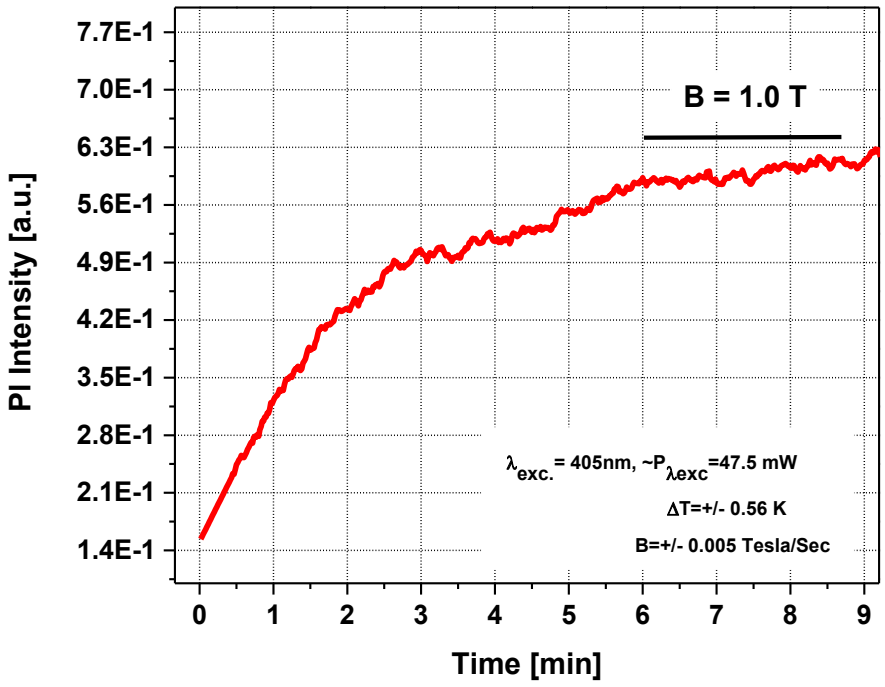

Figure 34. Shows the MO effect of the $KEu(WO_4)_2$, as a function of magnetization time, at a ramp rate of 5.0 [mTesla/sec], measured at T = 293 K, where B was held for 5 minutes.

From the obtained results, one can conclude that the sample exhibited a structural phase transition when magnetized, and that depends greatly on the magnetization time. As shown in the above figures, the sample final intensity remained higher than its initial one. Also, the Pl intensity had saturated and remained at its higher point.

Also, similar results were observed when switching direction of the magnetic field. Figure 35 shows the MO effect when applying the magnetic field in the opposite direction.

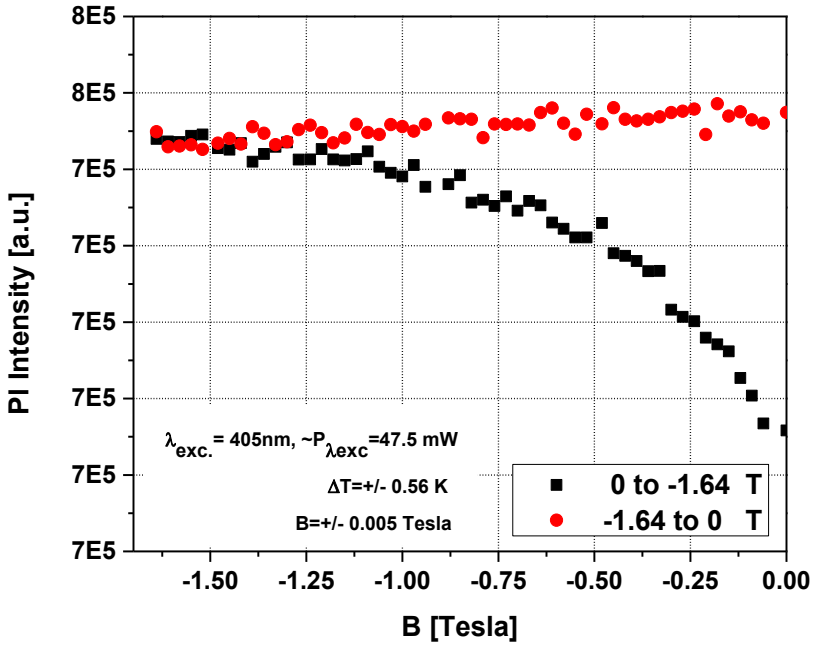

*Figure 35. Illustrates the longitudinal MO effect on $KEu(WO_4)_2$,as a function of magnetic field -**B**, at a ramp rate of 5.0 [mTesla/sec], measured at T = 293 K.*

An interesting results were observed as another experiment were conducted on a pre magnetized samples. The pre magnetized samples were placed between two permanent magnets under a magnetic field strength of ***B*** = 0.94 [Tesla] for 24 hours. The same experimental parameters that were used in magnetization time dependent experiment were used for observing the MO effect.

Figure 36 shows the MO effect of the pre-magnetized sample, and data from the previous experiment were used to compare the two. Also, on a new pre-magnetized sample.

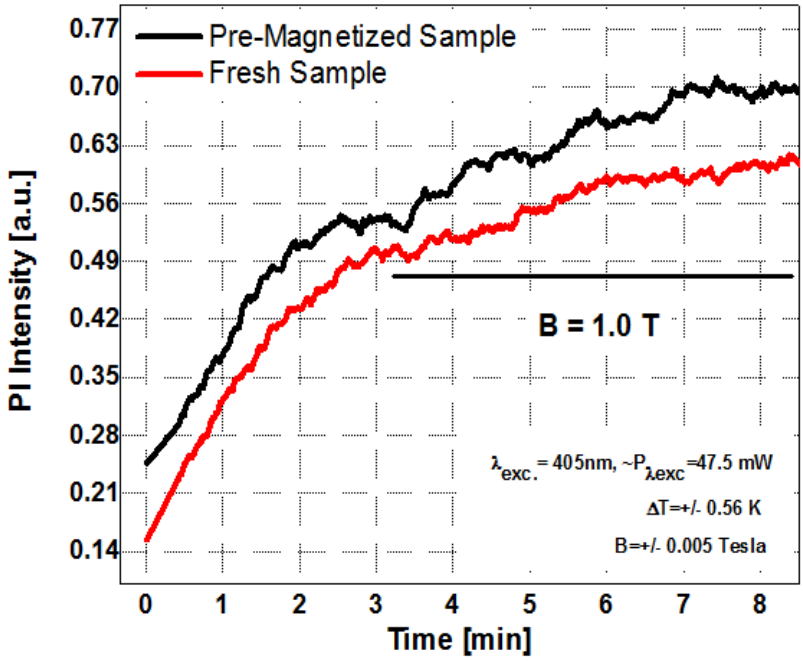

Figure 36. Illustrates the longitudinal MO effect on $KEu(WO_4)_2$,as a function of magnetization time. A pre-magnetized sample was used and previous results were used as a comparison. A ramp rate of 5.0 [mTesla/sec], measured at T = 293 K. ***B*** *held for 5 minutes.*

The results obtained above from the pre-magnetized sample showed a higher Pl intensity level than the starting point of the fresh sample. Pre-magnetizing the sample had enabled us to achieve a %15 higher Pl intensity level, and it had proved the structural phase transition phenomena in the material, which is a manifestation of the co-operative Jahn Teller effect. This phenomena was caused by the strong interaction between the electron spin in the *f* electron shell with the light photon energy, and by the presence of

quasi-degenerate ground state energy level in rare earth ions [43]. However, further research and measurements have to be investigated in order to additionally investigate the magnetization temperature dependency, and relaxation time on the $KEu(WO_4)_2$.

9. CONCLUSIONS

This project aimed at developing and upgrading the magneto-optical spectroscopy experimental setup, as well as the full understanding of the theory and characterization of the systems including upgrading the current Magneto-optical Kerr effect operated in the polar geometry using a new mirror based sample holder and two lock-in amplifiers for measuring the AC/DC signals simultaneously. The project also focused on constructing the Magnetic Circular Dichroism spectrometer for testing diluted magnetic semiconductors.

To test the upgraded MOKE spectroscopy, the a- AlN:Ni thin film test sample was used. The test samples had shown a great magneto optical effect in the recording of a Kerr spectrum and a Kerr hysteresis loop. These results confirmed the capability of our MOKE technique in the polar configuration in obtaining a Kerr hysteresis loop over the wide range of magnetic field.

The results generated from the GaMnAs/Sapphire thin film sample proved our newly developed MCD fully operational; as these results were comparable to those reported in [35]. It was also confirmed that MCD system is capable in recording an MCD spectrum along with an MCD hysteresis over the wide range of the magnetic field. The GaMnAs/InP structures were investigated as the research samples in the polar MCD configuration and the obtained results showed a ferromagnetic behavior.

In addition, the magneto-optical (MO) response/effect of the $KEu(WO_4)_2$ research samples in the longitudinal configuration was investigated. The samples have shown a great MO effect as an increase in the PL intensity under the presence of a magnetic field.

The effect of the $KEu(WO_4)_2$ was identified as the structural phase transition along with a Jahn-Teller effect in the rare earth compound due to magnetization.

In summary, a magneto-optical spectroscopy using MOKE and MCD techniques was designed and successfully built for various magneto-optical studies. The new configuration was able to obtain similar results to previous studies and can be utilized further.

10. FUTURE WORK

During the course of this project, many specific technical issues related to using equipment were successfully addressed and resolved. However, there were two main problems that this project didn't have the necessary equipment nor the test samples to address. First of all, since the scope of this project was construction and testing three different experiments and experimental setups, every experiment required using the same electromagnet, but with different experimental geometry. This obstacle limited the full automation of each experiment especially the MO spectroscopy, since MOKE and MCD have similar experimental setup. Therefore, I propose using a beam splitter to capture the light in the MO spectroscopy, this setup is explained in the following figure.

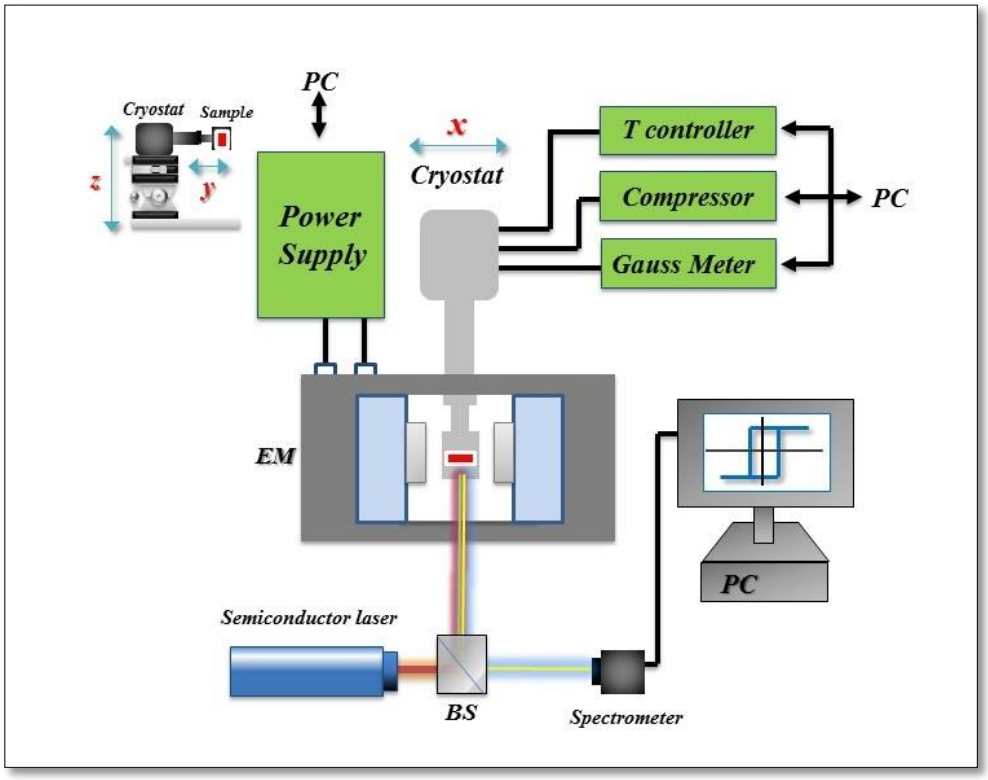

Figure 37. Illustrates using a Beam-splitter for the MO measurement.

The other problem that we faced during this project, was in the inability of utilizing the transmission mode geometry. In transmission mode geometry, a transparent sample is used and the magnetic field orientation is perpendicular to the sample surface. Typically, the optical bath in this geometry utilizes the electromagnet bores to guide the light. I have found this to be hard to optimize the optical alignment especially when using a lamp as a light source instead of a laser beam. Therefore, a new sample holder must be implemented by modifying the polar mirror sample holder that I implemented earlier. This will be using two mirrors placed within 45 degrees from each side of the sample. So, the light beam will reflect through the first mirror, then goes through the transparent

sample, and then reflect back to the detector using the second mirror. The Figure below illustrated the transmission mode double mirrors sample holder.

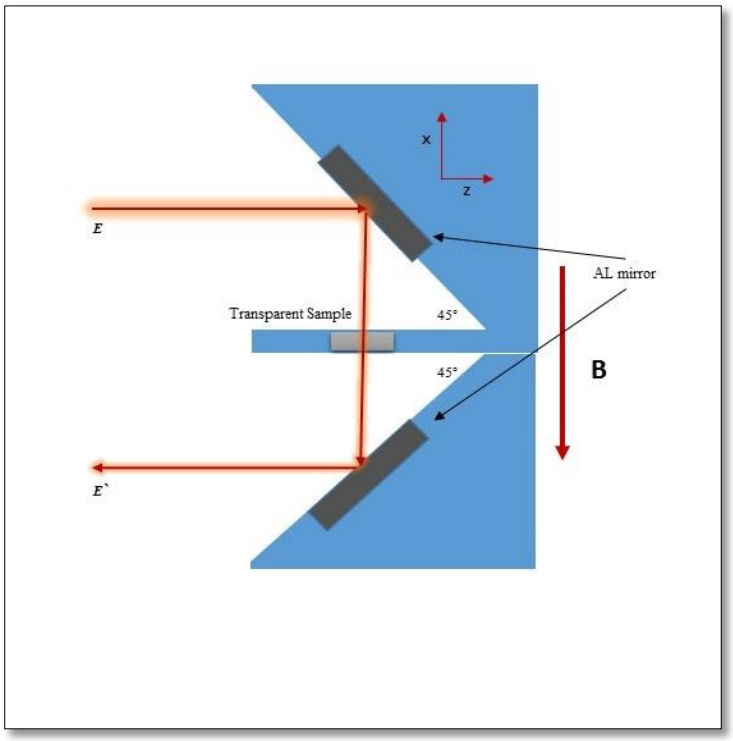

Figure 38. The Transmission Mode double mirrors sample Holder.

In summary, the two above ideas will be used as a part of the future work toward implementing and upgrading the experimental setup for various magneto-optical measurement.

REFERENCES

[1] K. Ando, S. Fujita, J. Ito, S. Yuasa, Y. Suzuki, Y. Nakatani, T. Miyazaki, and H. Yoda, "Spin-transfer torque magnetoresistive random-access memory technologies for normally off computing (invited)," *J. Appl. Phys.*, vol. 115, 2014.

[2] M. Johnson, "Spintronics.," *J. Phys. Chem. B*, vol. 109, pp. 14278–14291, 2005.

[3] K. Ando, *Magneto-Optics (Springer Series in Solid-State Sciences vol 128)*. Berlin: Springer, 2000.

[4] A. Khurshudov, *Magneto-optical storage system, the essiential guide to computer data storage*. Upper Saddle River, NJ: Prentice-Hall, 2001.

[5] H. Tanaka, "Development of MOKE Spectrometer for Magneto-optical Studies of Novel Magnetic Materials and Quantum Structures," Ohio University, 2008.

[6] E. R. Moog and S. D. Bader, "Superlattices and Microstructures," vol. 1, p. 543, 1985.

[7] S. Sarma, "A new class of device on the quantum of electron spin, rather than on charge, may yield the next generation of microelectronics," *Am. Sci.*, vol. 89, pp. 516–523, 2007.

[8] T. Maffitt, J. DeBrosse, J. Gabric, E. Grow, M. Lamorey, J. Parenteau, D. Willmott, M. Wood, and W. Gallagher, "Design considerations for MRAM," *IBM J. PRE, DEV*, vol. 50, no. 1, 2006.

[9] K. Aoshima, N. Funabashi, K. Machida, Y. Miyamoto, N. Kawamura, K. Kuga, N. Shimidzu, and F. Sato, "Spin transfer switching in current-perpendicular-to-plan spin valve observed by magneto-optical Kerr effect using visible light," *Appl. Phys. Lett.*, vol. 91, pp. 052507–1–052507–3, 2007.

[10] B. Lenth, "Optical Storage: a Growing Mass Market for Lasers," *Laser Focus Word*, vol. 44, p. 54, 2008.

[11] K. Ando, "Seeking Room-Temperature Ferromagnetic Semiconductors," vol. 312, no. June, pp. 1883–1885, 2006.

[12] M. Wakaki, *Optical Materials and Applications*. CRC Press, 2012.

[13] J. Gambino, *Intermetallic compounds and ferrites in Magneto-optical recording materiala*. Piscataway, NJ: IEEE press marketing, 2000.

[14] E. D. Palik, “A brief survey of magneto-optics,” *Appl. Opt.*, vol. 6, no. 4, 1967.

[15] M. Averous and M. Balkanaski, Eds., *Semimagnetic Semiconductors and Diluted Magnetic Semiconductors*. New York: Plenum, 1990.

[16] J. K. Furdyna, “Diluted magnetic semiconductors,” *J. Appl. Phys.*, vol. 64, no. R29, 1988.

[17] M. Jain, Ed., *Diluted Magnetic Semiconductors*. Singapore, 1991.

[18] R. Willardson and A. Beer, *Semiconductors and Semimetals*, Vol. 25. Boston, MA: Academic, 1988.

[19] R. Aggarwal, J. K. Furdyna, and S. von Molnar, Eds., “Diluted Magnetic (Semi-magnetic) Semiconductors,” *Mater. Res. Soc.*, vol. 89, 1987.

[20] K. Ando, “Electroc-Optics and Magneto-Optic Materials and Applications,” *SPIE 1126*, no. 58, 1989.

[21] J. Beltran-Huarac, J. Wang, H. Tanaka, W. M. Jadwisienczak, B. R. Weiner, and G. Morell, “Stability of the Mn photoluminescence in bifunctional ZnS:0.05Mn nanoparticles,” *J. Appl. Phys.*, vol. 114, no. 5, pp. 2–7, 2013.

[22] U. Valiev, J. Gruber, and G. Burdick, *Magnetooptical Spectroscopy of the Rare-Earth Compounds: Development and Application*. Scientific Research Publishing, Inc., 2012.

[23] G. A. Gehring, “Co-operative Jahn-Teller effects,” *Rep. Prog. Phys*, vol. 38, pp. 1–89, 1975.

[24] M. Galceran, M. C. Pujol, P. Gluchowski, W. Stręk, J. J. Carvajal, X. Mateos, M. Aguiló, and F. Díaz, “Synthesis, structural and optical characterization of Eu:KYb(WO4)2 nanocrystals: A promising red phosphor,” *Opt. Mater. (Amst).*, vol. 32, pp. 1493–1500, 2010.

[25] M. T. Borovets, Y. Kharchenko, T. Zayarnyuk, V. P. D’yakonov, M. Baranski, and H. Szymczak, “Spectroscopic and magnetic-optical properties of potassium-erbium double tungstate,” *J. Appl. Spectrosc.*, vol. 71, no. 5, pp. 709–714, 2004.

[26] a. K. Soika, I. T. Bodnar’, and I. O. Sologub, “A new magneto-optical effect in birefringent crystals doped with paramagnetic impurities,” *Opt. Spectrosc.*, vol. 112, no. 4, pp. 559–562, 2012.

[27] I. B. Krynetskiĭ, a. F. Popkov, a. I. Popov, M. T. Borowiec, a. Nabiałek, T. Zayarnyuk, and H. Szymczak, "First-order phase transition in potassium dysprosium tungstate induced by the field renormalization and softening of the elastic moduli in the vicinity of a structural Jahn-Teller-type transition," *Phys. Solid State*, vol. 48, no. 8, pp. 1553–1558, 2006.

[28] M. T. Borowiec, I. Krynetski, V. P. Dyakonov, a. Nabiałek, T. Zayarnyuk, and H. Szymczak, "Magnetostriction of rare earth double tungstates," *New J. Phys.*, vol. 8, 2006.

[29] M. T. Borowiec, "Anomalous properties of rare earth double tungstates," p. 4412, 2004.

[30] A. Arora, S. Ghosh, and V. Sugunakar, "A mirror based polar magneto-optical Kerr effect spectroscopy arrangement," *Rev. Sci. Instrum.*, vol. 82, 2011.

[31] and S. S. C. Hunt, "MOKE Magnifies Magnetic Moments [Magnificently!]," vol. 2, no. 2, p. 8, 1992.

[32] H. Magnan, "Surface Magneto-optic Kerr Effect." [Online]. Available: http://iramis.cea.fr/en/Phocea/Vie_des_labos/Ast/ast_sstechnique.php?id_ast=499. [Accessed: 22-Jan-2015].

[33] W. R. Mason, *a Practical Guide to Magnetic Circular Dichroism Spectroscopy*. Hoboken, New Jersey: Wiley, 2007.

[34] K. Ando, "Magneto-optical studies of s,p-d exchange interactions in GaN:Mn with room-temperature ferromagnetism," *Appl. Phys. Lett.*, vol. 82, no. 2003, pp. 100–102, 2003.

[35] H. Tanaka, W. M. Jadwisienczak, H. Saito, V. Zayets, S. Yuasa, and K. Ando, "Localized sp–d exchange interaction in ferromagnetic Ga 1− x Mn x As observed by magnetic circular dichroism spectroscopy of L critical points," *J. Phys. D. Appl. Phys.*, vol. 47, no. 355001, p. 355001, Aug. 2014.

[36] D. T. C. Oakberg, "Magneto-optic Kerr Effect," *Hinds Instruments*. [Online]. Available: http://www.hindsinstruments.com/techniques/moke/.

[37] C. You and S. Shin, "Derivation of simplified analytic formulae for magneto-optical Kerr effects," *Appl. Phys. Lett.*, vol. 69, no. June, pp. 1315–1317, 1996.

[38] H. Höchst, D. Rioux, D. Zhao, and D. Huber, "Directional magnetization effects in magnetic circular dichroism spectra of Fe," *Phys. Rev. B*, vol. 65, pp. 1–6, 2002.

[39] J. Qian and G. Wang, “A simple ultrahigh vacuum surface magneto-optic Kerr effect for the study of surface magnetic anisotropy,” *J. Vac. Sci.*, vol. A8, no. 6, pp. 4117–4119, 1990.

[40] A. Freeman and J. Ketterson, “Theoretical and Experimental Development of New Magneto-electronic Materials.” Department of physics, Northwestern University, 2145, Sheridan Road Evanston, IL, 60208.

[41] R. A. Hajjar, F. L. Zhou, and M. Mansuripur, “Magneto-optical measurement of anisotropy energy constants on amorphous rare-earth transition-metal alloys,” *J. Appl. Phys.*, vol. 67, no. 5328, 1990.

[42] H. Tanaka, W. M. Jadwisienczak, S. Kaya, G. Chen, C. Wan, and M. E. Kordesch, “Cluster and thickness dependence of ferromagnetism in nickel in situ-doped amorphous AlN thin films,” *J. Electron. Mater.*, vol. 42, no. 5, pp. 844–848, 2013.

[43] M. T. Borowiec, V. P. Dyakonov, K. Woźniak, Ł. Dobrzycki, M. Berkowski, E. E. Zubov, E. Michalski, a Szewczyk, M. U. Gutowska, T. Zayarnyuk, and H. Szymczak, “Crystal structure and magnetic properties of potassium erbium double tungstate KEr(WO 4) 2,” *J. Phys. Condens. Matter*, vol. 19, no. 5, p. 056206, 2007.

[44] S. Polisetty, J. Scheffler, S. Sahoo, Y. Wang, T. Mukherjee, X. He, and C. Binek, “Optimization of magneto-optical Kerr setup: Analyzing experimental assemblies using Jones matrix formalism,” *Rev. Sci. Instrum.*, vol. 79, 2008.

APPENDIX A. DERIVATION OF EQUATIONS FOR KERR ROTATION AND KERR ELLIPTICITY FOR THE MIRROR POLAR MOKE GEOMETRY USING REFLECTING MIRROR

This section describes the analytical derivation for the MOKE spectroscopy in the polar geometry using the 45° mirror sample holder.

For the analysis, Jones matrix will be the main mathematical approach for deriving and understanding the Kerr rotation and Kerr ellepticity for the polarized waves.

First of all, the reflected electric field vector of the incident linearly polarized light at angle Θ, which is relative to the *x-z* plane is represented by

$$E'(\Theta) = |E| \begin{pmatrix} \cos(\Theta) \\ \sin(\Theta) \end{pmatrix} \quad A.1$$

It is also important to keep in mind the jones matrix representations of each optical component. Therefore, we start off by the Jones matrix representation for the Polarizer ***P***, and the analyzer ***A***, with their major transmission axis oriented at their angles β, and α, respectively. [44]

$$\hat{P}(\beta) = \begin{bmatrix} cos^2\beta & \sin\beta\cos\beta \\ \sin\beta\cos\beta & sin^2\beta \end{bmatrix} \quad A.2$$

$$\hat{A}(\alpha) = \begin{bmatrix} cos^2\alpha & \sin\alpha\cos\alpha \\ \sin\alpha\cos\alpha & sin^2\alpha \end{bmatrix} \quad A.3$$

Since the signal is modulated by the Photo-elastic modulator (PEM-100). The PEM is represented by the jones matrix with its modulation axis at the x-z plane below.

$$\widehat{PEM}(\varphi) = \begin{bmatrix} exp^{i\varphi/2} & 0 \\ 0 & exp^{-i\varphi/2} \end{bmatrix} \quad A.4$$

Where $\varphi = \varphi_0 \cos(2\pi f t)$, is the sinusoidally varying retardation angle generated by the PEM. The incident beam is then reflected on the sample surface by the mirror surface at angle δ. The sample equation is presented by the Fresnel reflection matrix, and the mirror is presented by the normalized jones matrix [30]

$$\hat{S} = \begin{bmatrix} r_{pp} & r_{ps} \\ r_{sp} & r_{ss} \end{bmatrix} \quad A.5$$

$$\widehat{M}(\delta) = \begin{bmatrix} \tan \Psi(\delta)\, exp^{i\Delta(\delta)} & 0 \\ 0 & 1 \end{bmatrix} \quad A.6$$

Where r_{ij} is the ratio between the incident (*s,* and *p* polarized lights), and the reflected polarized light. $\Psi(\delta)$, and $\Delta(\delta)$ are the ellipsometry parameters of the mirror. Keeping in mind that δ_1 is the incident reflected beam, where δ_2 is the reflected electric field by the sample surface.

For near normal angle of incident $r_{ss} = r_{pp}$, therefore, equation A.6 of the sample becomes

$$\hat{S} = \begin{bmatrix} r_{pp} & r_{ps} \\ r_{sp} & r_{pp} \end{bmatrix} \quad A.7$$

Then by taking r_{pp} out, it becomes

$$\hat{S} = r_{pp} \begin{bmatrix} 1 & r_{ps}/r_{pp} \\ r_{sp}/r_{pp} & 1 \end{bmatrix} \quad A.8$$

Since, we are trying to obtain the Kerr rotation $\emptyset_K$, and Kerr ellipticity ε_K parameters, the relationship between r_{sp}/r_{pp} is the way to obtain them.

$$\frac{r_{sp}}{r_{pp}} = \emptyset_K + j\varepsilon_K \qquad A.9$$

$$\frac{r_{ps}}{r_{pp}} = -(\emptyset_K + j\varepsilon_K) \qquad A.10$$

As a result, the sample jones matrix becomes

$$\hat{S} = r_{pp}\begin{bmatrix} 1 & -(\emptyset_K + j\varepsilon_K) \\ \emptyset_K + j\varepsilon_K & 1 \end{bmatrix} \qquad A.11$$

The reflected electric field at the detector is obtained by the dot product of all the optical components, and their jones matrix representation is

$$\begin{aligned} \vec{E_D} &= \hat{A}(90°)\cdot\hat{M}(\delta_2)\cdot\hat{S}\cdot\hat{M}(\delta_1)\cdot\widehat{PEM}(\varphi)\cdot E'(-45°) \\ &= \begin{bmatrix} cos^2 90° & \sin 90°\cos 90° \\ \sin 90°\cos 90° & sin^2 90° \end{bmatrix}\cdot\begin{bmatrix} \tan\Psi(\delta_2)\, exp^{i\Delta(\delta_2)} & 0 \\ 0 & 1 \end{bmatrix}\cdot \\ &\quad \left[r_{pp}\begin{bmatrix} 1 & -(\emptyset_K + j\varepsilon_K) \\ \emptyset_K + j\varepsilon_K & 1 \end{bmatrix}\right]\cdot\begin{bmatrix} \tan\Psi(\delta_1)\, exp^{i\Delta(\delta_1)} & 0 \\ 0 & 1 \end{bmatrix}\cdot \\ &\quad \begin{bmatrix} exp^{\frac{i\varphi}{2}} & 0 \\ 0 & exp^{-\frac{i\varphi}{2}} \end{bmatrix}\cdot\left[\,|E|\begin{pmatrix}\cos(-45°)\\ \sin(-45°)\end{pmatrix}\right] \\ &= \frac{|E|}{\sqrt{2}}\, exp^{-\frac{i\varphi}{2}}\begin{bmatrix} 0 \\ -1 + exp^{i(\varphi+\Delta(\delta_1))}\tan\Psi(\delta_1)\,(\emptyset_K + j\varepsilon_K) \end{bmatrix} \end{aligned} \qquad A.12$$

The above was solved using Matlab symbolic solve function.

Since the δ_2 is the angle in which the reflected light from the sample surface into the surface of the Al mirror doesn't appear, that means, the Al mirror doesn't have any effect on the polarization of electric field.

The measured intensity of the reflected light ***I*** at the detector can be expressed by

$$I = \grave{E}_D^* E_D \qquad A.13$$

$$\grave{E}_D^* = \frac{|E|}{\sqrt{2}} exp^{+\frac{i\varphi}{2}} \begin{bmatrix} 0 \\ -1 + exp^{-i(\varphi+\Delta(\delta_1))} \tan\Psi(\delta_1)\,(\emptyset_K + j\varepsilon_K) \end{bmatrix} \qquad A.14$$

$$\grave{E}_D^* E_D = \left[\frac{-|E|}{\sqrt{2}} e^{+\frac{i\varphi}{2}} + \frac{|E|}{\sqrt{2}} e^{-i(\frac{\varphi}{2}+\Delta(\delta_1))} * \tan\Psi(\delta_1)\,(\emptyset_K + j\varepsilon_K)\right]$$

$$\cdot \left[\frac{-|E|}{\sqrt{2}} e^{-\frac{i\varphi}{2}} + \frac{|E|}{\sqrt{2}} e^{-i(\frac{\varphi}{2}-\Delta(\delta_1))} * \tan\Psi(\delta_1)\,(\emptyset_K + j\varepsilon_K)\right]$$

$$= \frac{|E^2|}{2}(1) - \frac{|E^2|}{2} e^{+i\Delta(\delta_1)} * \tan\Psi(\delta_1)\,(\emptyset_K + j\varepsilon_K) - \frac{|E^2|}{2} e^{-i(\varphi-\Delta(\delta_1))}$$

$$* \tan\Psi(\delta_1)\,(\emptyset_K + j\varepsilon_K) + \frac{|E^2|}{2} e^{-i\varphi} * (\tan\Psi(\delta_1)\,(\emptyset_K + j\varepsilon_K))^2$$

$$= \frac{|E^2|}{2}\big[1 - e^{+i\Delta(\delta_1)} * \tan\Psi(\delta_1)\,(\emptyset_K + j\varepsilon_K) - e^{-i(\varphi-\Delta(\delta_1))}$$

$$* \tan\Psi(\delta_1)\,(\emptyset_K + j\varepsilon_K) + e^{-i\varphi} * (\tan\Psi(\delta_1)\,(\emptyset_K + j\varepsilon_K))^2\big]$$

$$= \frac{|E^2|}{2}\big[1 - \tan\Psi(\delta_1)\,(\emptyset_K + j\varepsilon_K) * \big(cos\Delta(\delta_1) + isin\Delta(\delta_1)\big)$$

$$- \tan\Psi(\delta_1)\,(\emptyset_K + j\varepsilon_K) * \big(\cos\big(\varphi + \Delta(\delta_1)\big) - isin\big(\varphi + \Delta(\delta_1)\big)\big)$$

$$+ (\tan\Psi(\delta_1)\,(\emptyset_K + j\varepsilon_K))^2(\cos\varphi - isin\varphi)\big]$$

$$= \frac{|E^2|}{2}\big[1 - 2\tan\Psi(\delta_1)\,(\emptyset_K * \cos\big(\varphi + \Delta(\delta_1)\big) + \emptyset_K * isin\big(\varphi + \Delta(\delta_1)\big) + j\varepsilon_K$$

$$* \cos\big(\varphi + \Delta(\delta_1)\big) - \varepsilon_K * sin\big(\varphi + \Delta(\delta_1)\big)\big] \qquad A.15$$

Due to the lock-in amplifier view technique, only the lowest Fourier components of the equation A.15 are acceptable and in interest for the sake of the measurement, as a result, the equation is reduced to become the following

$$I = \frac{|E^2|}{2}\big[1 - 2\tan\Psi(\delta_1)\,(\emptyset_K * \cos\big(\varphi + \Delta(\delta_1)\big) - \varepsilon_K * sin\big(\varphi + \Delta(\delta_1)\big)\big] \qquad A.16$$

The expression $\frac{|E^2|}{2}$ is the wavelength dependent source intensity, and the detector response, and it can be expressed by I_0 , as a result equation A.16 becomes

$$I = I_0\big[1 - 2\tan\Psi(\delta_1)\,(\emptyset_K * \cos\big(\varphi + \Delta(\delta_1)\big) - \varepsilon_K * sin\big(\varphi + \Delta(\delta_1)\big)\big] \qquad A.17$$

The above expression can be expressed in the Bessel function form using the following Bessel function expansion formulas

$$\sin(\varphi_0\, cos(2\pi ft)) = 2J_1\varphi_0 \cos(2\pi ft) + \cdots$$

$$\cos\big(\varphi_0 cos(2\pi ft)\big) = J_0(\varphi_0) - 2J_1(\varphi_0)\cos(4\pi ft) + \cdots \quad A.18$$

Therefore,

$$I_{DC} = 1 + 2tan\Psi J_0(\varphi_0)(\emptyset_K cos\Delta(\delta_1) - \varepsilon_K sin\Delta(\delta_1) \quad A.19$$

$$I_f = 4tan\Psi J_1(\varphi_0)(\varepsilon_K cos\Delta(\delta_1) + \emptyset_K sin\Delta(\delta_1)) \quad A.20$$

$$I_{2f} = 4tan\Psi J_2(\varphi_0)(-\varepsilon_K sin\Delta(\delta_1) + \emptyset_K scos\Delta(\delta_1)) \quad A.21$$

Where I_f , and I_{2f} , are the detector signal from the PEM-100 modulation at the modulation frequency of *f*, and its second harmonic *2f*. The AC lock-in amplifier measures the AC signal of the *f*, and *2f*, and the second DC lock-in amplifier measures the I_{DC}.

So, we can re-write equation A.17 as

$$I = I_0\big[I_{DC} + I_f\cos(2\pi ft) + I_{2f}\cos(4\pi ft) + \cdots\big] \quad A.22$$

At a retardation angle set at the PEM where $\varphi_0 = 2.405$, we can obtain $J_0(\varphi_0) = 0$, and we can obtain the following relationships for the ac and the dc signals.

$$\frac{I_f}{I_{DC}} = 2\sqrt{2}J_1(\varphi_0)\big(\varepsilon_K cos\Delta(\delta_1) + \emptyset_K sin\Delta(\delta_1)\big)tan\Psi \quad A.23$$

$$\frac{I_{2f}}{I_{DC}} = 2\sqrt{2}J_2(\varphi_0)(-\varepsilon_K sin\Delta(\delta_1) + \emptyset_K scos\Delta(\delta_1)\, tan\Psi \quad A.24$$

It is also important to keep in mind, that the lock-in amplifier for the AC measurement, measures the root-mean square, which means that the above expression include a factor o f$\frac{1}{\sqrt{2}}$. That implies to the strong fusing of the corresponding signal due to the Kerr rotation $\emptyset_K$, and Kerr ellipticity ε_K parameters over the mirror's ellipsomtery parameters; $tan\Psi$, and Δ.

We can assume the following mirror's ellipsomtery parameters in the absence of the mirror where $tan\Psi = 1,$ and $\Delta = 0$. Therefore, equations A.23, and A.24 can be simplified to

$$\frac{I_f}{I_{DC}} = 2\sqrt{2}AJ_1(\varphi_0)\varepsilon_K \qquad A.25$$

$$\frac{I_{2f}}{I_{DC}} = 2\sqrt{2}BJ_2(\varphi_0)\emptyset_K \qquad A.26$$

From the above expression, we are able to obtain the Kerr rotation $\emptyset_K$, and Kerr ellipticity ε_K parameters.

APPENDIX B. LABVIEW GRAPHICAL USER INTERFACE (GUI)

This section describes the main front panels of the LabVIEW code, in this project, we have used LabVIEW ver. 12.0, which was used to remotely control the experiment for both MOKE and MCD. This code was used to obtain and display both the MOKE, and the MCD spectrum, it was also used to display the final plots of a hysteresis loop.

The LabVIEW code consists of a front panel graphical user interface (GUI) that controls the physical instruments that is used for the experiment. The front panel of the GUI consisted of knobs, push buttons, switches, numerical parameters for inputs/outputs values. Each physical commercial instrument that was used to run the experiment has a developed, and a modified process in the LabVIEW code to remotely control the experiment. Those instruments are listed below.

For controlling the magnetic field, we used a DC power supply (LakeShore, model # 642), and a Gauss meter (LakeShore, model # 475 DSP) for monitoring the magnetic field. A lock-in amplifier (Stanford Research, model # SR830) was used for obtaining the AC, and the DC signal for the spectrum and the hysteresis loop. A photo-elastic modulator (Hinds Instrument, model # PEM-100) was used for modulating the signal at a specific frequency, optimized by the user and the front panel interface. Finally, for scanning over a specific spectral range, a monochromator (mode # CM110) was used. The physical instruments have a LabVIEW driver code, and a GUI that have been modified for the experiments.

B-1 DC power supply GUI

Figure B- 1 shows the front panel of the DC power Supply GUI. The hysteresis loop is measured in a three-loop process. Each loop goes through twenty increments for measuring a given section of the hysteresis loop. The number of loops defines the averaging of one segment in the loop. The ramping rate is used to ascent and decent the DC current. Once the operator determines the number of loops, increments, ramping rate, and maximum current, the loop is automatically calculated.

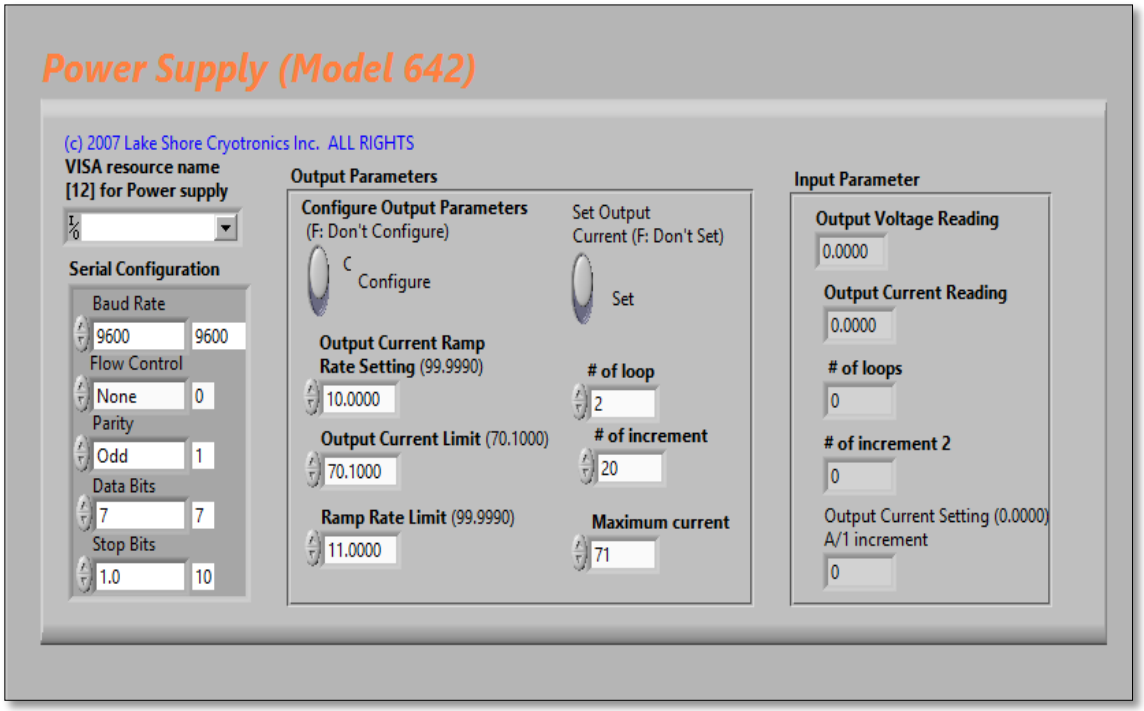

Figure B- 1. The front Panel of DC power supply.

B-2 CM110 MONOCHROMATOR GUI

The front panel of the CM110 monochromator is used for obtaining the MOKE and MCD spectrum. The front panel of the monochromator enables the user to scan over the any specific spectral range. The code will start scanning over the spectrum range once the operator determine the starting wavelength using this code, and the final wavelength using the Photo Elastic Modulator (PEM) panel. Figure B- 2 illustrates the front panel of the CM110 monochromator GUI.

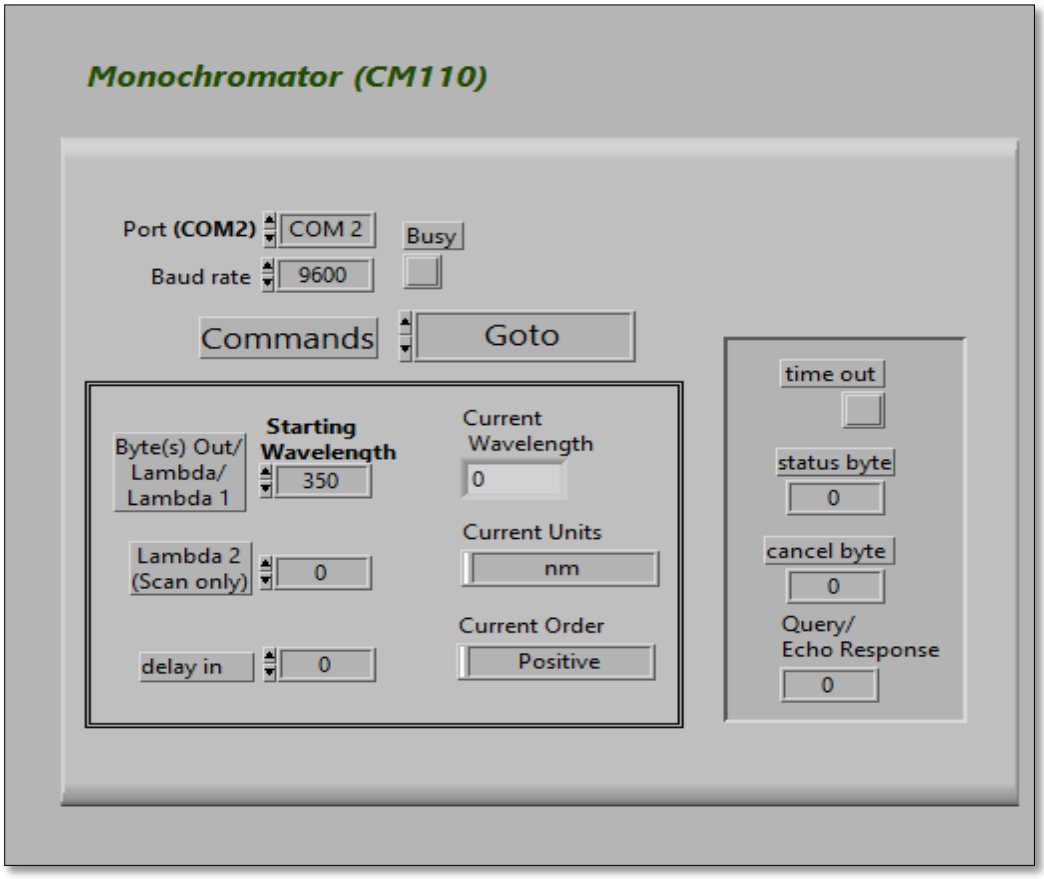

Figure B- 2. The front panel of the CM110 monochromator.

B-3 PHOTO-ELASTIC MODULATOR (PEM-100) GUI

The front panel of the PEM0-100 is used to modulate the signal at a specific wavelength and frequency. This GUI is used when scanning over a spectral range. That is done be specifying the starting and ending wavelength, and the increments for each step. Figure B- 3 shows the front panel GUI of the PEM-100.

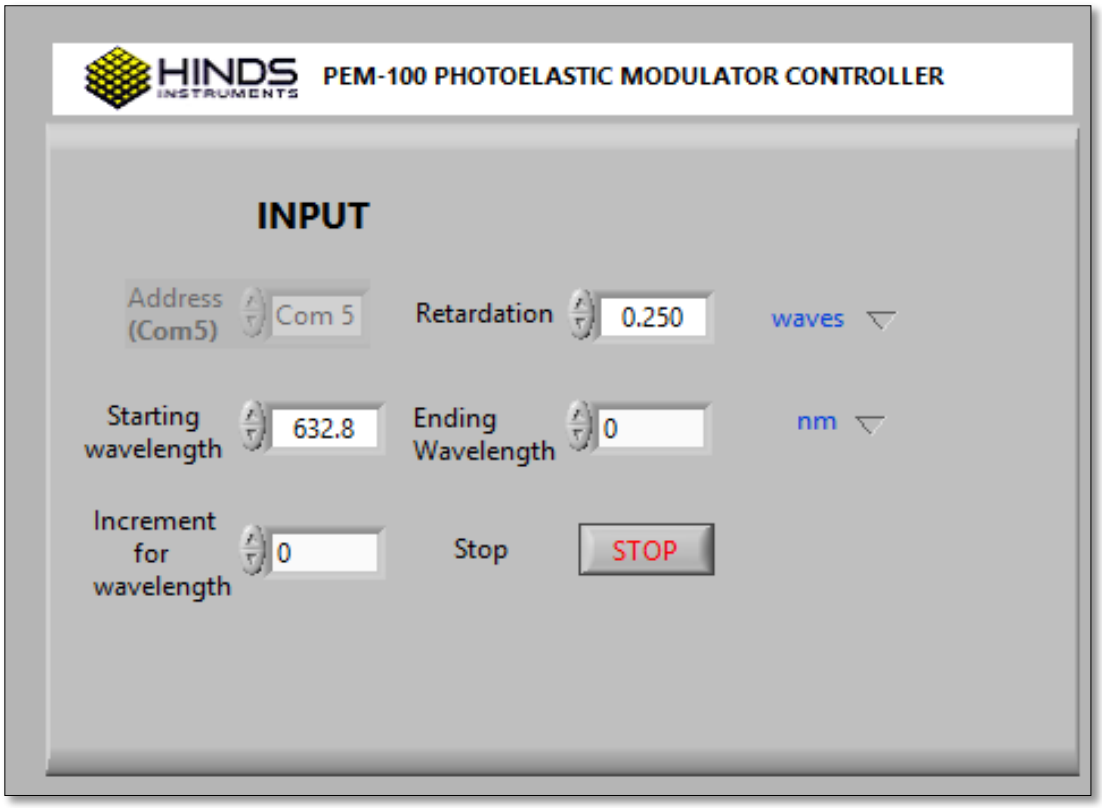

Figure B- 3. The front panel of the Photo-Elastic Modulator (PEM-100) controller.

B-4 GAUSSMETER (475 DSP) GUI

The front panel of the gaussmeter (LakeShore, model # 475 DSP) GUI is used for monitoring, displaying, and plotting the magnetic field parameter. The user can choose

the magnetic field unit, in our case, we choose Tesla as the main unit for all the measurements. Figure B- 4 shows the front panel GUI of the gauss meter.

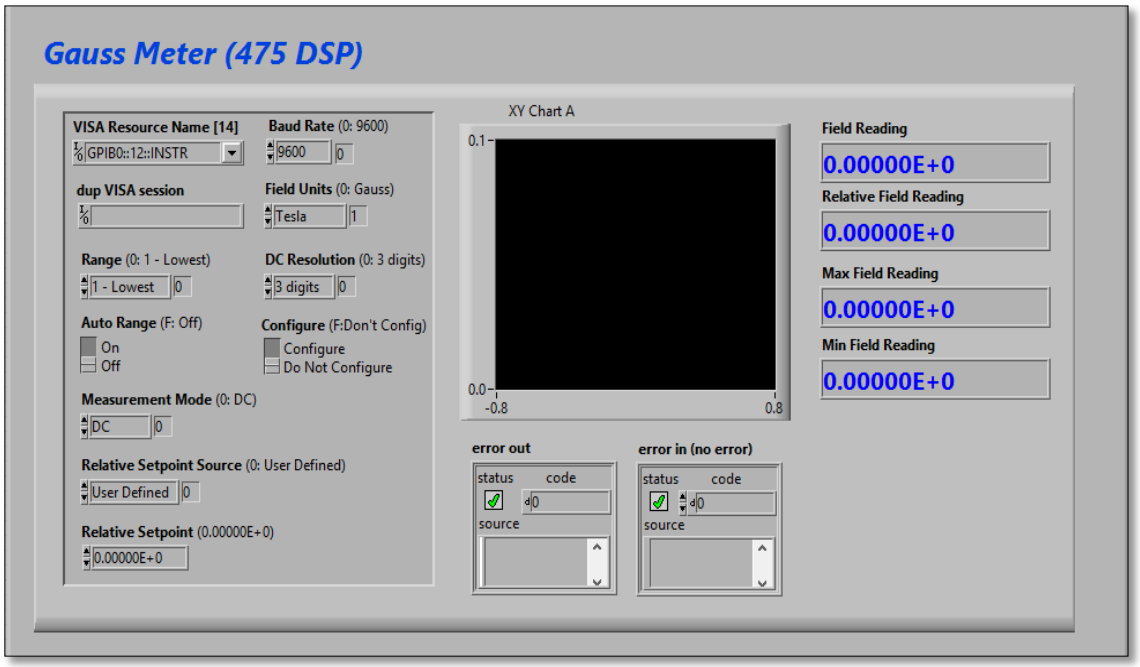

Figure B- 4. The front panel of the Gaussmeter GUI

B-5 LOCK-IN AMPLIFIER GUI

The lock-in amplifier GUI controls several parameters in the experiment for both the AC, and the DC measurement. The user must define main parameter, including AC, or DC coupling, sensitivity, time constant, slop, and the reference phase. Figure B-5 and Figure B-6 illustrate the lock-in amplifier GUI for the AC, and the DC signal respectively.

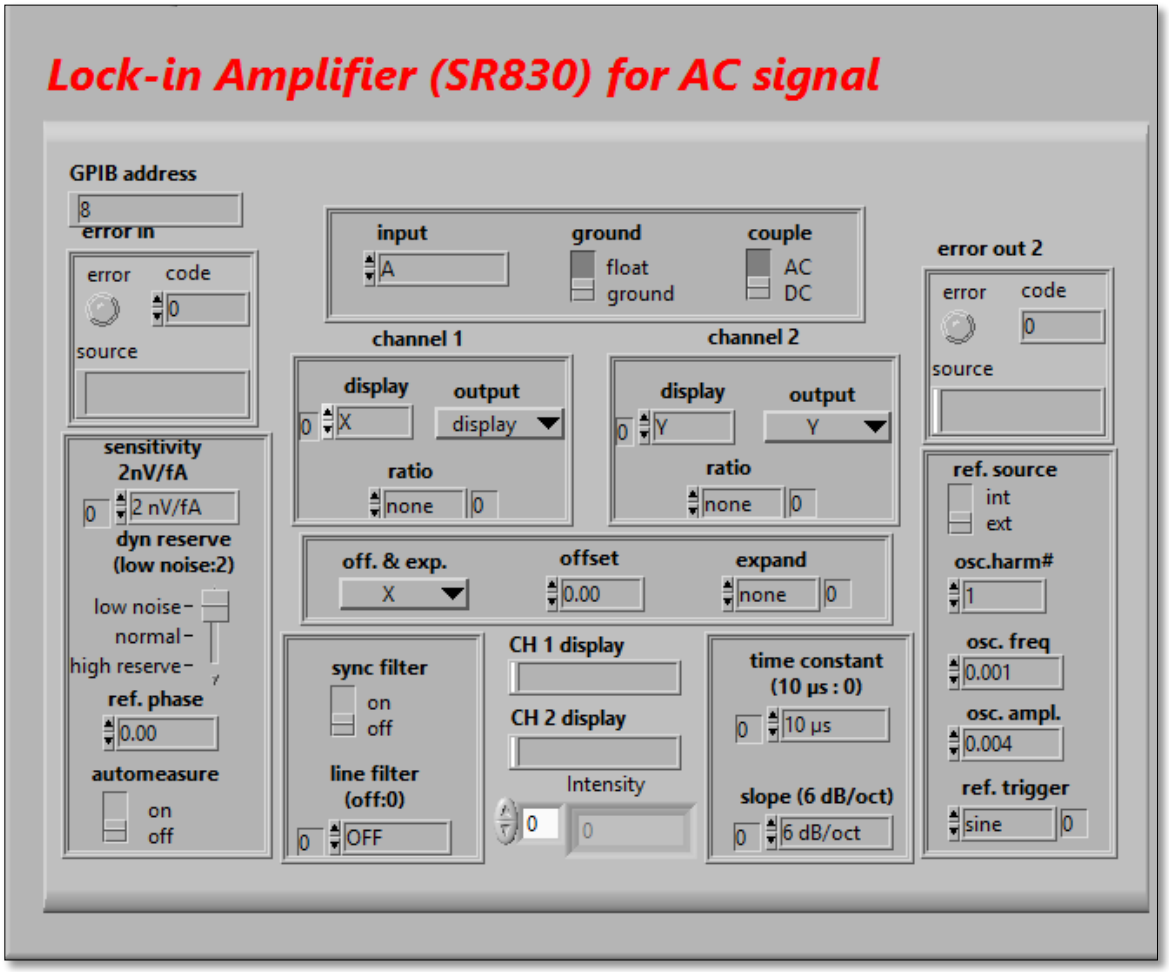

Figure B- 5. The front panel of the Lock-in amplifier for AC signal GUI

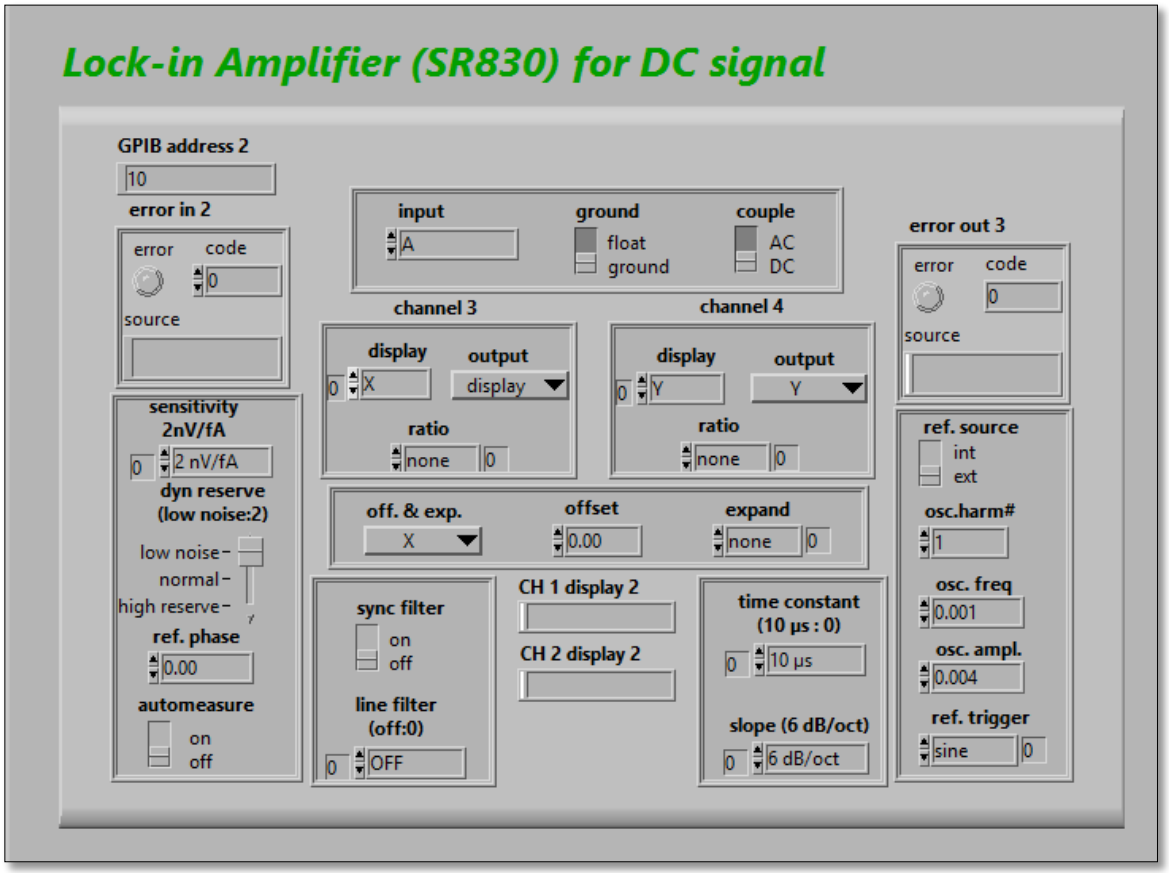

Figure B- 6. The front panel of the Lock-in amplifier for DC signal GUI

Thesis and Dissertation Services